universität wien

MASTERARBEIT / MASTER'S THESIS

Titel der Masterarbeit / Title of the Master's Thesis

„Development of 3D bioprinted fibrin-alginate scaffolds for 3D culture of adipose tissue derived mesenchymal stem cells"

verfasst von / submitted by

Maja Maver

angestrebter akademischer Grad / in partial fulfilment of the requirements for the degree of

Master of Science (MSc)

Wien, 2022 / Vienna 2022

Studienkennzahl lt. Studienblatt / degree programme code as it appears on the student record sheet:	UA 066 830
Studienrichtung lt. Studienblatt / degree programme as it appears on the student record sheet:	Master's degree programme Molecular Microbiology, Microbial Ecology and Immunobiology
Betreut von / Supervisor:	Assist. Prof. Robert Woodward

Table of Contents

List of Figures

List of Tables

ACKNOWLEDGEMENTS

First, I would like to thank my supervisor at the University of Vienna, Assistant Professor Robert Woodward, who, although following my master's thesis from afar, was very motivating and supportive throughout the entire process.

I would also like to express my gratitude to my mentor at the University of Maribor, Associate Professor Uroš Maver. His support and understanding inspired and motivated me throughout my Master's thesis. In addition to his scientific knowledge, I would not have been able to complete this thesis without his warm gestures welcoming me to the new environment and inspiring me to pursue the field of biomedical engineering.

I would also like to express my deep gratitude to Dr. Boštjan Vihar, who guided me throughout the work and broadened my horizons. I am very grateful to him for his encouragements, without which this thesis would not have been the same. He introduced me to the team of experts, all of whom have been very supportive and whose friendship I will cherish forever.

Last but not least, I would like to express my gratitude to my husband and my entire family. I thank them from the bottom of my heart for giving me the strength to overcome even the hardest days and for their supportive words that encouraged me to never give up.

ABSTRACT

Tissue engineering aims to develop functional bioartificial tissues for use in regenerative medicine and drug screening. In the last decade, the field of tissue engineering has been transformed by three dimensional (3D) printing technologies that aim to recreate geometrically well-defined structures or scaffolds as precursors of native tissues and develop them into *in vitro* models of tissues, organs and diseases. The scaffolds are platforms for 3D cell culture, allowing cells to proliferate and develop in an environment that more closely resembles natural tissues, compared to traditional two dimensional (2D) cell culture substrates. Due to their biocompatible properties, low toxicity and good degradability, hydrogels made of various synthetic or natural polymers are mostly used in tissue engineering for fabrication of scaffolds. In this study, biomaterial inks composed of 1% alginate and 1% fibrinogen respectively, were used for scaffold fabrication using extrusion based 3D printing within a support bath. In addition, adipose tissue-derived mesenchymal stem cells were added to the hydrogel. The developed “bioink” and printing process showed a high degree of biocompatibility while allowing controlled degradation. Finally, comparative cell culture results show higher overall metabolic activity of cells cultured within the scaffolds, compared to cells cultured on the scaffold surface. This showcases the potential of the developed bioink and 3D printing protocol for the development of *in vitro* tissue and disease models based on mesenchymal stem cells.

GERMAN ABSTRACT

Gewebekonstruktion (engl. Tissue Engineering) zielt darauf ab, funktionelles bioartifizielles Gewebe für den Einsatz in der regenerativen Medizin und im Arzneimittelscreening zu entwickeln. In den letzten zehn Jahren wurde das Gebiet der Gewebekonstruktion durch dreidimensionale (3D) Drucktechnologien verändert, die darauf abzielen, geometrisch genau definierte Strukturen oder Gerüste (engl. scaffolds) als Vorläufer nativer Gewebe nachzubilden und sie zu In-vitro-Modellen von Geweben, Organen und Krankheiten zu entwickeln. Die Scaffolds sind Plattformen für 3D-Zellkultur, die es Zellen ermöglichen, sich in einer Umgebung zu vermehren und zu entwickeln, die natürlichem Gewebe ähnlicher ist als herkömmliche zweidimensionale (2D) Zellkultursubstrate. Aufgrund ihrer biokompatiblen Eigenschaften, geringen Toxizität und guter Abbaubarkeit werden Hydrogele aus verschiedenen synthetischen oder natürlichen Polymeren im Tissue Engineering oft zur Herstellung von Scaffolds verwendet. In dieser Studie wurden Biomaterialtinten aus 1 % Alginat und 1 % Fibrinogen für die Gerüstherstellung unter Verwendung von extrusionsbasiertem 3D-Druck in einem Trägerbad verwendet. Zusätzlich wurden dem Hydrogel mesenchymale Stammzellen aus Fettgewebe zugesetzt. Das entwickelte „Bioink“- und Druckverfahren zeigte ein hohes Maß an Biokompatibilität und ermöglichte gleichzeitig einen kontrollierten Abbau. Schließlich zeigen komparative Zellkulturergebnisse eine höhere metabolische Gesamtaktivität von Zellen, die innerhalb der Gerüste kultiviert werden, im Vergleich zu Zellen, die auf der Gerüstoberfläche kultiviert werden. Dies zeigt das Potenzial des entwickelten Bioink- und 3D-Druckprotokolls für die Entwicklung von *in vitro* Gewebe- und Krankheitsmodellen auf der Grundlage mesenchymaler Stammzellen.

1. INTRODUCTION

1.1 Tissue engineering

Tissue engineering (TE) is an interdisciplinary field that aims to develop a bioartificial tissue to repair damaged tissue, create disease models, and for drug screening by combining biology and engineering knowledge [Walles and Walles, 2011]. According to organdonor.gov, there are currently more than 106,000 people on the waiting list for an organ transplant in the United States [Organdonor, 2022]. In addition, the organization states that 17 people die each day waiting for an organ transplant. Even if an organ transplant occurs, the implanted organ may be rejected by the host's immune system or it may cause an adverse reaction that can be fatal [Ravindranath et al., 2021]. These risks and the statistics behind them make it imperative to advance the development of artificial tissues that overcome the limitations of not being patient-specific or suppressed by the immune system.

The beginnings of the development of materials for TE date back to the late 1960s, when Wichterle and Lim used hydrogels to make soft contact lenses and suggested that they might be biocompatible because they did not irritate the eyes [Wichterle and Lim, 1960]. Over the next few years, additional studies were conducted predicting that with advances in biocompatible materials, new tissues could be generated by seeding cells onto a suitable scaffold [Evans et al., 2006]. In the mid-1990s, a first stereolithography device was developed by Chuck Hull and used for two-dimensional (2D) cell deposition [Hull, 1984], and more than a decade later, the first human stem cells were isolated [Shamblott et al., 1998]. It was a breakthrough at TE, when in 1999 the first human organ, a bladder, was printed three-dimensionally (3D) from synthetic building blocks and grown in the laboratory, then coated with host bladder cells and implanted [Atala et al., 2006], further expanding the capabilities of TE. In 2002, the first extrusion-based bioprinter was introduced [Lander et al., 2002], and two years later, the first tissue consisting of cells only, without scaffolds, was 3D bioprinted [Jakab et al., 2004]. Since then, 3D printing has been used on TE for various biomedical applications, which are described in the following sections.

1.1.1 Principles of tissue engineering

The general principle of TE is to either culture the cells in the laboratory or isolate them from the donor, further culture them in the presence of specific growth factors to trigger their proliferation, combine them with a biocompatible material to support their growth, and finally implant the tissue construct into the patient (Figure 1) [Saroia et al., 2018].

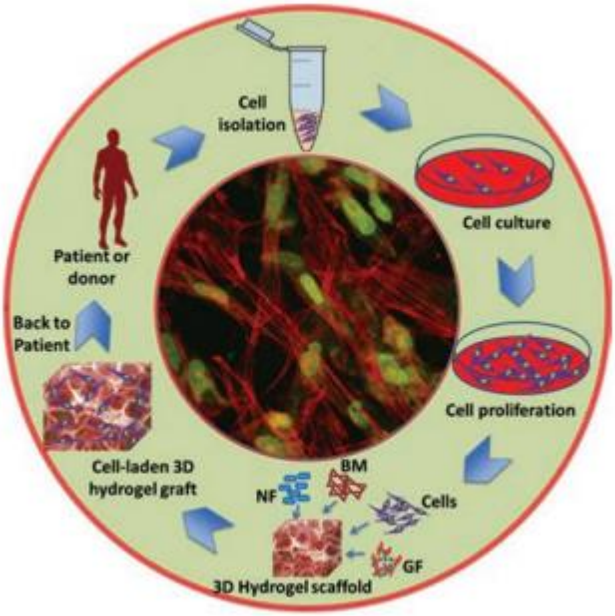

Figure 1. The operating principle of tissue engineering [Rana et al., 2014]

TE can be based on spheroids, self-assembling 3D cell aggregates formed by cell-cell and cell-matrix interactions that mimic tissue [Chae et al., 2021], or scaffolds, a support structure made of synthetic or natural polymers, possibly mixed with cells and growth factors, engineered to contribute to cell growth and functional tissue formation [Gomillion and Burg, 2011]. In this Master's thesis, the focus is on scaffold-based TE.

There are three essential elements of scaffold-based TE: 1) a scaffold made of a biomaterial (hereafter referred to as material) that provides an environment for cell or tissue growth, 2) growth factors or bioreactors that not only mechanically support the spheroid or scaffold but also provide a suitable chemical environment for tissue development, and finally 3) cells or tissues themselves that can be grown on these scaffolds *in vitro* [Saroia et al., 2018].

1.2 Hydrogel scaffolds

Normally, cells are grown in a laboratory in a plastic or glass Petri dish. However, the growth conditions in a Petri dish do not mimic the natural cell environment well [Caliari and Burdick, 2016]. In fact, 2D cell culture systems are not a good representative of an actual 3D environment in a natural tissue for several reasons [Baker and Chen, 2012]. First, cells in a Petri dish are generally flattened and tend to lose their differentiated phenotype. Moreover, cells growing in a single layer communicate only with their neighboring cells, which is not the case in the *in vivo* environment where cross-communication between different cell layers can be observed. As a result, signaling is altered and cell polarity can be disrupted.

To overcome the limitations of a 2D culture, hydrogels have been introduced and are widely used because they support cell adhesion and cell signaling between different cell layers and

mimic the mechanics of soft tissue [Tibbit and Anseht, 2009]. Hydrogels are polymeric materials with hydrophilic properties that enable them to retain large amounts of water, which is possible due to functional groups with hydrophilic properties attached to the polymeric backbone [Song et al., 2021]. A hydrogel used for cell culture is called a scaffold. A hydrogel scaffold provides a supportive mechanical structure for tissue development [El-Sherbiny and Yacoub, 2013]. Cells can either be suspended within the 3D scaffold of the hydrogel or cultured and attached to its surface. Ideally, a hydrogel scaffold provides only temporary support for the cells until they establish their own extracellular matrix (ECM) [Murphy and Atala, 2014]. The ECM is a 3D network, usually composed of proteins such as collagen and elastin, glycoproteins, enzymes, and other molecules, with the role of providing structural support and a suitable biochemical environment for the surrounding cells [Theocharis, 2016]. In addition, the components of the ECM enable cell adhesion and intracellular communication.

1.2.1 Types of hydrogels

One way to categorize hydrogels is based on their origin, that is, whether the material from which they are made is synthetic or natural. Synthetic polymers are used to synthesize synthetic hydrogels, including polyglycolic acid, polyethenglycol, and polyamides [Gyles et al., 2017]. The main advantage of synthetic materials is their mechanical strength, high availability, and consistency between monomers [Saroia et al., 2018]. However, it is difficult to degrade them under the physiological microenvironment, which is their main disadvantage [Song et al., 2021]. Synthetic polymers such as polylactic acid and polyglycolic acid have been used for the engineering of bone, nerve, skin, and other tissues at TE [Dhandayuthapani, 2011].

Natural hydrogels are made from naturally occurring polymers that are highly biocompatible and biodegradable and promote high cell attachment. However, it is difficult to ensure uniform composition and material properties within a batch, which is their major drawback [Saroia et al., 2018]. Some natural polymers include collagen, gelatin, and hyaluronic acid (HA) from ECM, alginate from marine algae or seaweed, fibrin from blood, and chitosan from crustaceans [Gyles et al., 2017]. The variety of bonds, which can be easily modified, make collagen one of the most commonly used natural proteins for the preparation of hydrogels [Dinescu et al., 2018]. It can form sponges, be mixed with other polymers, and strongly resembles ECM. Thanks to these properties, it has been used to make artificial skin [Tangsadthakun et al., 2017], cartilage [Lee et al., 2001], spinal cord [Joosten et al., 2004], and others. Gelatin also has great properties such as easy degradability and biocompatibility [Saroia et al., 2018].

1.2.2 Properties of hydrogels

To ensure the success of scaffold-based TE and create a tissue that closely resembles native tissue and allows the formation of ECM, a material for hydrogel fabrication must have the desired properties. These include biocompatibility or non-cytotoxicity of the material to the cells, biodegradability, suitable viscosity, cross-linking capabilities (if required), and more [Rana et al., 2014].

The hydrogels used in this work were selected for their ease of printing and properties that make them suitable for cell culturing.

The first criterion for selecting a hydrogel is its viscosity, which is particularly important if that hydrogel is to be used for 3D printing, as described in detail in Section 1.3. A low viscosity hydrogel is mechanically weak and cannot produce a structure with a defined geometry [Murphy and Atala, 2014]. In addition, mechanical strength is important to provide support for the cells while they build their own ECM.

The mechanical strength of the scaffold can be increased by increasing the concentration of the material used, combining a low viscosity hydrogel with another more viscous material, or inducing cross-linking [Chen et al., 2017]. Cross-linking involves connecting polymer chains together, creating a stabilized network structure that transforms a liquid polymer into a solid gel, a process known as gelation [Maitra and Shukla, 2014]. The cross-linking process can occur either through the formation of covalent bonds or ionic bonds [Rana et al., 2014]. Chemical cross-links include chemical reactions, irradiation, radicals, and enzymes. An example of a chemically cross-linked biomaterial is fibrinogen, a natural blood-derived polymer that is enzymatically cross-linked to fibrin by the addition of thrombin (more on this in Section 1.3.3). Although chemical cross-linking offers better mechanical properties, it can be toxic as it generates free radicals and toxic ions that could affect cell viability.

Physical cross-linking, on the other hand, does not release potentially toxic chemicals, but it does result in lower mechanical strength. These include pH and temperature changes, hydrogen bonding, ion and protein interactions, and others. Alginate is an example of a biomaterial that requires the addition of divalent cations for gelation and was used in this project [Gasperini et al., 2014]. Gelatin can also be physically cross-linked by adjusting the temperature of the gel. At temperatures below body temperature, gelatin is solid, but when the temperature rises to 37°C, it becomes water-soluble, making 3D scaffolds composed only of gelatin quite unstable.

Another very important property of a hydrogel relates to cell growth and includes biocompatibility, degradation rate, and cell attachment [Murphy and Atala, 2014].

First, a biocompatible hydrogel does not produce a cytotoxic substance that could significantly decrease the viability of cells encapsulated in it or cultured on its surface [Murphy and Atala, 2014]. Furthermore, if the tissue is to be transplanted into the patient, it is important that the

hydrogel does not induce an undesirable immunogenic response in the host [Naahidi et al., 2017].

Second, hydrogels should be degradable. Structurally, hydrogels only provide mechanical support for cells until they establish their own ECM. Degradation of hydrogels can then occur through cell-mediated proteases, which is the case for natural hydrogels such as collagen and fibrin [Caliari and Burdick, 2016], or through the breaking of bonds formed during cross-linking, as in alginate. It is very important to note that TE aims to produce hydrogels whose rate of degradation is proportional to the rate of regeneration of new tissue or ECM, and that the degradation process itself should not produce wastes that could be potentially toxic to cells [Ozeki and Tabata, 2012].

Third, hydrogels should also allow cell-matrix interactions. Due to its hydrophilicity, alginate does not provide good cell-matrix interaction [Lee and Mooney, 2012], making it more difficult for cells to grow and proliferate within the hydrogel scaffold than with fibrin, to which cells can attach more easily. To ensure cell attachment in hydrogels with poor attachment properties, some chemical modifications can be made, such as introducing certain functional groups into the gel surface [Lee et al., 2019].

The following table summarizes the source, type, cross-linking method required for gelation, and main advantages and disadvantages of the three natural polymers used in this master's thesis: alginate, fibrin and gelatin.

Tabel 1: **Natural hydrogels used in this thesis and their properties** [Leberfinger et al., 2017]

Material	Source	Cross-linking method	Advantages	Disadvantages
Alginate	Seaweed	Physical – ionic reaction	- Fast gelation - Inexpensive - Good mechanical stability	- Poor cell attachment due to high hydrophilicity - Limited long-term stability
Fibrin	Blood	Chemical – enzymatic reaction Physical – ionic reaction	- Promotes angiogenesis - Controllable degradation - Low risk of immunogenic reactions (can be produced from patient`s blood)	- Poor mechanical stability - Easily clogs
Gelatin	ECM	Physical – thermal	- Reversible gelation - Promotes cell attachment	- Poor mechanical stability - Short degradation time

1.2.3 Cell-laden hydrogels

When cells are encapsulated in a cross-linked framework of a hydrogel scaffold, the hydrogel is referred to as cell-laden [Blaeser et al., 2017]. A typical cell-laden hydrogel is prepared by mixing a cell suspension with a prepolymer solution and then applying one of the previously described cross-linking methods to initiate gelation [Rana et al., 2014]. It is important to use non-invasive cross-linking methods, such as the addition of an enzyme like thrombin in the case of fibrinogen or the addition of $CaCl_2$ in the case of alginate, to protect the cells. Since molecules such as thrombin and $CaCl_2$ are already present in the native tissue environment, they usually do not harm the cells.

Cell-laden hydrogels have been used by researchers for cartilage tissue engineering [Snyder et al., 2014], chondrogenic differentiation [Liu et al., 2010], spinal cord injury repair [Hong et al., 2017], neural cell tissue engineering [Abelseth et al., 2019], [Montgomery et al., 2015], organoid printing [Zhang et al., 2016], cardiac tissue engineering [Pena et al., 2018), and more.

In this work, a hydrogel of alginate and fibrinogen was mixed with adipose-derived mesenchymal stem cells (ADMSC), as described in more detail in the following section.

1.2.3.1 ADMSC

Human mesenchymal stem cells (hMSC) are multipotent adult stem cells that can be derived from various tissues [Abdallah and Kassem, 2008]. Adipose-derived mesenchymal stem cells (ADMSC), for example, are non-hematopoietic MSCs derived from adipose tissue found in various parts of the body, such as under the skin, around organs and blood vessels, and even between muscles. Like all other stem cells, ADMSCs have self-renewal potential through division and can differentiate into adipocytes, chondrocytes, and osteocytes or into pancreatic endocrine progenitor cells [Doering et al., 2019].

MSCs have already been used in combination with various hydrogels. For example, they were grown on a chitosan-based hydrogel and used in the acute kidney injury study, where they showed some therapeutic benefits [Choe et al., 2012]. In another study, gelatin-based hydrogels were shown to promote differentiation of ADMSC into chondrocytes. [Salamon et al., 2014]. In combination with fibrinogen, MSCs were used in a study by Kisiday et al. (2011). In this study, MSCs distributed more evenly on fibrinogen-rich protein (FRP) surfaces than on tissue culture plastic surfaces, suggesting that FRP may accelerate cell proliferation.

In their study, Aliborzi et al. (2016) showed that ADMSC have very favorable growth kinetics with a population doubling time of about 60 hours, making them very suitable candidates for research in TE. Moreover, in the same study, it was observed that ADMSC maintained a typical fibroblast-like morphology for 8 passages, after which the proliferation rate started to decrease. In addition, the presence of cell surface markers for MSC (CD44 and CD90) and the absence of hematopoietic markers (CD43) were detected during 8 passages. Finally, ADMSC showed successful differentiation toward adipogenic and osteogenic lineages 3 weeks after

differentiation induction. In another study [Su et al., 2018], the rate of ECM protein production by ADMSC was measured. The results showed that ADMSC grown on 3D polycaprolactone could produce major ECM proteins including collagen type I and III, decorin, tenascin, and tenomodulin within 14 days, which is an important aspect when considering the degradation rate of a hydrogel scaffold on which ADMSC are grown.

1.3 3D- printing and -bioprinting

As mentioned earlier, it is desirable to fabricate a scaffold of hydrogel or cell-laden hydrogel with a defined geometry. To achieve this, the 3D printing process can be used. 3D printing is an additive process in which a 3D construct is formed by successively depositing material layer by layer. The result is a 3D shape with complex geometry that can be used in a variety of applications from high-volume manufacturing to personalized medicine [Murphy and Atala, 2014].

The beginnings of 3D printing date back to 1986, when Chuck Hull printed his first 3D structure by depositing thin layers of material using a method he called "sterolithography" [Hull, 1986]. The field continued to evolve to printing a 3D scaffold directly from biological material and using it in transplantation procedures [Nakamura et al., 2010]. Finally, 3D printing with cells was introduced and given a name that is still used today - 3D bioprinting [Zopf et al., 2013].

Similar to 3D printing, 3D bioprinting is an additive process of successive, layer-by-layer, precise deposition of material, with the difference that 3D bioprinting specifically uses a material that contains cells [Murphy and Atala, 2014]. The 3D structure produced has a well-defined geometry and spatial positioning of the cells.

1.3.1 Extrusion-based 3D (bio)printing technology

The choice of 3D bioprinting technology depends on the material used for printing, its properties, and whether or not the hydrogel is mixed with cells during the printing process. In this thesis, an extrusion-based technique was used.

Extrusion-based technique is a nozzle-based technique and includes mechanical screw-driven, piston-driven, and pneumatic-driven systems [Murphy and Atala, 2014]. The syringe used in this system can be filled with biomaterial or bioink and is extruded through the nozzle via one of three mechanisms - mechanical screw, piston, or pneumatic system (Figure 2).

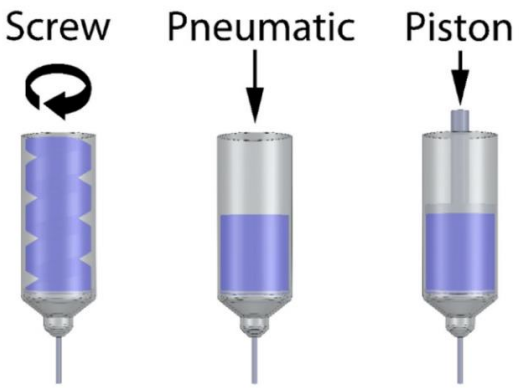

Figure 2. Three mechanisms used in nozzle-based bioprinting technique
[Derakhshanfar et al., 2018]

The mechanical screw mechanism, which was also used in this thesis, rotates the special screw to extrude the material and is especially used in printing high viscosity hydrogels [Derakhshanfar et al., 2018]. The main drawback is the pressure exerted by the screw, which can damage the cells and affect their viability.

The pneumatic mechanism requires air under pressure to extrude the material and has the advantage over the other two mechanisms in that it has the least impact on cell viability. However, its main disadvantage lies in the control system [Murphy and Atala, 2014]. Namely, there is a time delay after the air is compressed to the point where the material is actually extruded.

The third mechanism, the piston-based one, overcomes the disadvantage of the pneumatic mechanism by establishing a direct contact between the surface pressed on the material by a piston and the material itself [Murphy and Atala, 2014]. Therefore, the extrusion process can be easily controlled and the pressure is continuous.

The extrusion-based technique is only suitable for viscous liquids [Murphy and Atala, 2014]. Therefore, the most commonly used materials in this technique are collagen, alginate and fibrinogen. The fact that they are liquid when they exit the nozzle makes it difficult for the researcher to obtain a specific shape. To overcome this, materials can be printed in support baths (the details of which are described in the following section), such as fibrinogen in a gelatin support bath, or they can be combined with a less viscous material before printing [Hinton et al., 2015]. In addition, materials such as alginate can be cross-linked with $CaCl_2$ immediately after the extrusion process to maintain shape and provide better mechanical properties [Siti et al., 2019].

1.3.1.1 Freeform Reversible Embedding of Suspended Hydrogels (FRESH)

To overcome the low viscosity and thus low mechanical strength of some materials such as fibrinogen, a support bath can be used in which the 3D-printed construct is embedded [Hinton et al., 2015]. This approach, which was also used in this thesis, is referred to as the FRESH method.

FRESH is a method that first gained attention in 2015 when Hinton et al. (2015) printed structures in a temporary support with thermoreversible and biocompatible properties. Printing these structures from materials with a Young's modulus of less than 500 kPa at a resolution of approximately 200 µm would otherwise be very difficult to achieve.

The main advantage of FRESH is that a 3D construct is printed in the bath without changing the position of the construct. The needle can still move freely through the bath without breaking the geometric shape or causing cracks [Shiwarski et al., 2021]. Each time the needle moves, it displaces the fluid and deposits the material. The most commonly used material for the support bath is gelatin, but materials such as alginate [Pallegrino et al., 2021] or Pluronic-F127 [Afghah et al., 2020] can also be used. When fibrinogen is printed into a gelatin support bath, the gelatin can be mixed with thrombin prior to printing to allow cross-linking [Hinton et al., 2015]. Fibrinogen can also be printed into gelatin using the FRESH method if it has been previously mixed with cells, as shown in Figure 3.

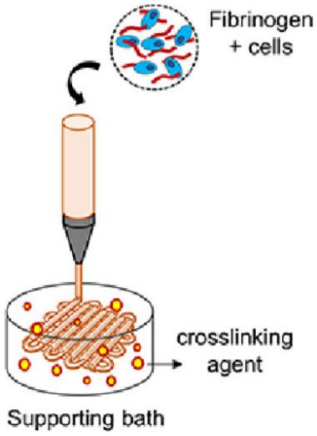

Figure 3. FRESH method for 3D bioprinting fibrinogen with cells [de Melo et al., 2020]

1.3.2 Inks and bioinks

It is important to distinguish whether the hydrogel used in 3D printing contains only the material itself or whether it is also mixed with a specific type of cell. Hydrogels that contain only the material, whether it is natural or synthetic, are referred to as inks [Groll et al., 2018]. On the other hand, hydrogels that are also mixed with cells are called cell-laden hydrogels or bioinks.

In this project, the focus is on alginate and fibrinogen, two natural polymers used to make an ink and a bioink hydrogel.

1.3.2.1 Alginate

Alginate is a salt of alginic acid. It is a natural polymer formed by the combination of linear copolymers of β-D-mannuronic acid and α-l-guluronic acid found in polysaccharides of brown algal species such as *Ascophyllum* and *Durvillaea* [Alihosseini, 2016]. The copolymers give alginate its mechanical strength and flexibility, making it an ideal candidate for the preparation of hydrogels where high viscosity and stability are required [Angra et al., 2021]. 100 years after its discovery, in the 1980s, alginate was first used in wound dressings due to its high ability to absorb water and its potential to produce gels [Qin, 2004]. Namely, when ions are exchanged between alginate fibres and blood, optimal moisture and temperature conditions for wound healing can be achieved [Thomas et al., 2000].

Alginate forms hydrogels with multivalent cations such as Ca^{2+}, Ba^{2+}, and Fe^{3+}, which bind between the chains of the guluronate blocks and form a 3D gel-like network [Mishra, 2015]. The model is called an "Egg-box" model due to its shape (Figure 4).

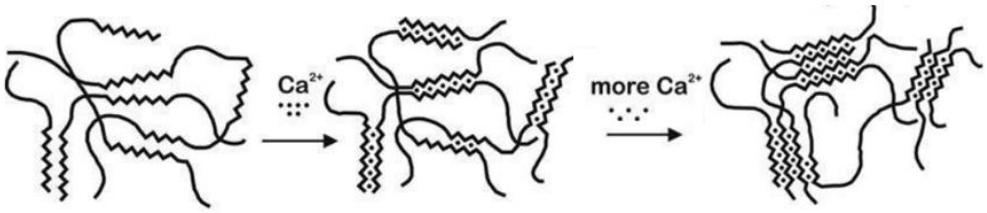

Figure 4. The "Egg-box" model of alginate forming a gel [Mishra, 2015]

Hydrogels made from alginate are not only mechanically strong, which is very important for 3D printing applications, but have also been shown to be biocompatible [Gibas and Janik, 2010] and biodegradable. Alginate can be degraded with alginase, an enzyme that cleaves a glycosidic bond [Lee and Mooney, 2012]. Pure alginate is not degradable in mammals because the enzyme alginase is not present. However, ionically cross-linked alginate gel can be dissolved by ion exchange and can therefore be used as an implant material in *in vivo* applications, where it is naturally degraded by the exchange of ions present in the body [Lueckgen et al., 2019].

All the above properties make alginate an ideal candidate for use in TE. The following table summarizes some studies in which alginate was used in combination with different cell types for the production of hydrogels and 3D printing.

Tabel 2. Some studies on 3D bioprinting of alginate bioinks

Bioink composition	3D bioprinting method	Cross-linking method	Application in biomedicine	Reference
Alginate with mouse fibroblasts	Inkjet printing into CaCl2 support solution	$CaCl_2$	Vascular-like cellular structures	[Christensen et al., 2015]
Alginate, GelMA[2] and PEGTA[3] with HUVECs[4]	Coaxial extrusion-based	$CaCl_2$ and photocrosslinking	Perfusable vascular structure	[Jia et al., 2016]
Alginate with MSC	Extrusion-based	$CaCO_3$, $CaCl_2$, or $CaSO_4$	Controlled growth factor delivery	[Freeman and Kelly, 2017]
Alginate with hMSC	Pneumatic extrusion-based	$CaCl_2$ or $CaSO_4$	Anatomically accurate bone grafts	[Fernandez et al., 2021]
Alginate and GelMA with cardiac endothelial cells	Extrusion-based	$CaCl_2$ and photocrosslinking	Cardiac patches for epicardial transplantation	[Gentile, 2021]

1.3.2.2 Fibrinogen

Fibrinogen is a polymer found in blood plasma that is best known for its role in blood clotting [Walker and Royston, 2002]. When a tissue is injured and bleeding begins, platelets aggregate to activate clotting and initiate the formation of a clot. This process is catalyzed by thrombin, which is produced from prothrombin by a series of enzymatic reactions (Figure 5). Thrombin cleaves the N termini of the alpha and beta chains of fibrinogen, which are then stabilized by factor XIIIa in the presence of Ca^{2+} ions. This irreversible polymerization reaction forms a fibrin clot that is now capable of triggering the healing cascade in which the remaining immunogenic cells are activated to completely heal the damaged tissue [de Melo et al., 2020].

[2] Gelatin methacryloyl (GelMA)
[3] Poly(ethylene glycol)-tetra-acrylate (PEGTA)
[4] Human umbilical vein endothelial cells (HUVECs)

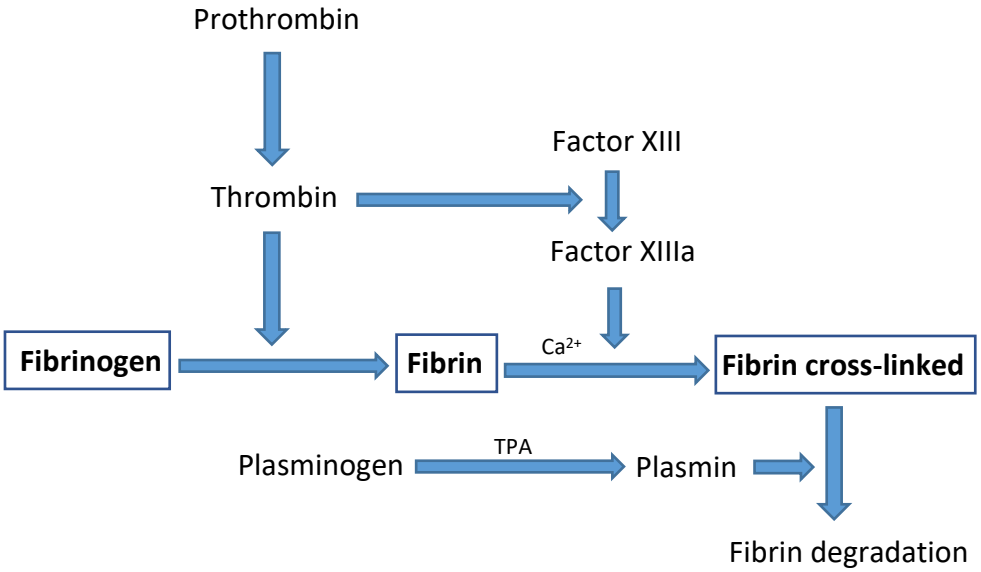

Figure 5. The process of fibrin formation from fibrinogen during blood coagulation[5]

Once the tissue is healed, the fibrin clot must be dissolved. This is done by the process of fibrinolysis, in which plasminogen is activated by tissue plasminogen activator (TPA) [Thelwell and Longstaff, 2007]. Plasminogen is then converted to plasmin, which is attracted to and dissolves the fibrin clot (Figure 5).

The property of being biodegradable makes fibrin an excellent candidate for the preparation of hydrogels. In addition, fibrin's structure makes it a very suitable natural polymer for hydrogels. Namely, it contains amino acids such as arginine, glycine, and aspartic acid, all of which are suitable for cell attachment, a crucial aspect in selecting a hydrogel scaffold to which cells can successfully attach and proliferate [Laurens et al., 2006].

Overall, fibrin is an excellent candidate for the preparation of hydrogels in 3D bioprinting and as a scaffold for 3D cell culture due to its biocompatible properties, high cell attachment, biodegradability, and ease of preparation and handling. The following table summarizes some studies in which fibrinogen was used as a bioink with different cell types in 3D bioprinting.

[5] The figure has been created by Word Illustrations.

Tabel 3. Some studies on 3D bioprinting of fibrinogen bioinks

Bioink composition	3D bioprinting method	Crosslinking method	Application in biomedicine	Reference
Fibrinogen, gelatin and hMSCs	Extrusion-based	Chemical with PEG[6]	Mimetic and customizable tissue and organ constructs	[Rutz et al., 2015]
Fibrinogen with gelatin, alginate and HGSC[7]	Extrusion-based	Transglutaminase for gelatin, Ca^{2+} for alginate	Brain tumor model for drug susceptibility	[Dai et al., 2016]
Fibrinogen with human smooth muscle cells	Drop-on-demand with sacrificial gelatin	Thrombin	*In vitro* blood vessel model	[Schöne-berg et al., 2018]
Fibrinogen with hMSC spheroids	Extrusion-based with PEG and alginate in support bath with thrombin supplement	UV-light for PEG, Ca^{2+} for alginate and thrombin for fibrin	Mimetic cartilaginous tissues that support locomotion	[de Melo et al., 2019]
Fibrinogen with GelMA and HUVECs[8]	Extrusion-based with acoustic nozzle for cell excitation and alignment	UV-light for GelMA	Vascular network performance and functionality improvement	[Sriphut-kiat et al., 2019]

Like any other hydrogel, fibrin gel has its pitfalls. Apart from being quite expensive, its main drawback is that it is very soft and cannot maintain its shape when extruded through the 3D printer [Laurens et al., 2006]. The viscosity of fibrinogen does not change when shear forces change, so the printed structure collapses immediately and does not solidify until it is cross-linked with thrombin.

Several solutions have been proposed to maintain the shape of the fibrinogen during printing and to obtain optimal layer-by-layer and mechanically stable constructs.

One of these solutions, namely printing into a support bath, has already been described in Section 1.3.1.1. Another solution is mixing fibrinogen with another biomaterial such as polyethylene glycol (PEG). In the study by Rutz et al. (2015), a gel mixture of fibrinogen and polyethylene glycol with two reactive groups (PEGX) was prepared and printed in cuboid form using a pneumatic 3D printer. The printed construct was self-supporting, thick, and retained the morphology layer by layer.

Fibrinogen can also be combined with alginate, which is described in more detail in the following section.

[6] Polyethylene glycol (PEG)
[7] Human glioma stem cells (HGSC)
[8] Human umbilical vein endothelial cells (HUVECs)

1.3.2.3 Alginate and fibrinogen hydrogels

Alginate and fibrinogen each have their advantages and disadvantages when used as hydrogels for the fabrication of bioink 3D scaffolds. The following figure shows the positive contributions of the two hydrogel materials in producing a hydrogel with the best properties.

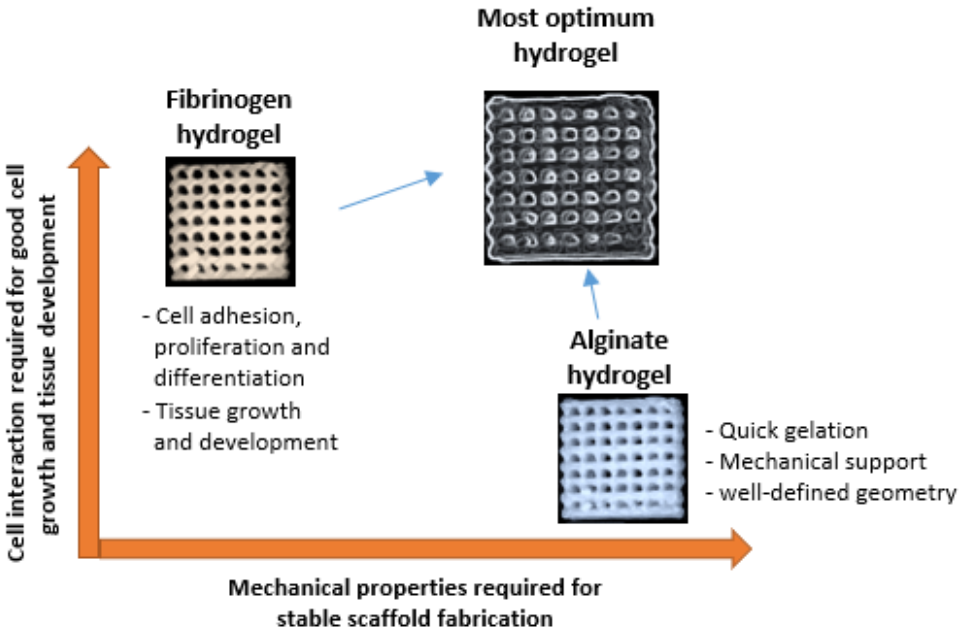

Figure 6. Properties of fibrin and alginate required for hydrogel fabrication with the best properties.[14]

[14] The figure has been created by Word Illustrations.

Some studies that attempted to combine alginate with fibrinogen for 3D printing of a scaffold are summarized in Table 4.

Tabel 4. Some studies using alginate and fibrinogen hydrogels as bioinks

Hydrogel composition	Cross-linking method	Application in biomedicine	Reference
Gelatin/alginate/fibrinogen with neuron cells and Schwann cells	$CaCl_2$ and thrombin	*In vitro* reproduction of nerve fibers	[Li et al., 2009]
Gelatin/alginate/fibrinogen with hepatocytes	$CaCl_2$ and thrombin	Vascularized liver	[Li et al., 2009]
Gelatin/alginate/fibrinogen with ADSC	$CaCl_2$ and thrombin	Vascularized adipose tissues	[Xu et al., 2009]
Gelatin/alginate/fibrinogen matrix with ADSC[15]	$CaCl_2$ and thrombin	*In vitro* physiological model of the metabolic syndrome	[Xu et al., 2010]
Gelatin/alginate/fibrinogen/ PU[16] with ADMSC	$CaCl_2$ and thrombin	Branched vascular template implants	[Huang et al., 2013]
Gelatin/alginate/fibrinogen with Hela cells	$CaCl_2$ and thrombin	*In vitro* cervical tumor model	[Zhao et al., 2014]
Alginate/fibrin with ADMSC	$CaCl_2$ and thrombin	*In vitro* osteogenic differentiation for *in vivo* treatment of bone wounds	[Grzesiak et al., 2015]
Gelatin/alginate/fibrinogen with ADMSC and hepatocytes	$CaCl_2$ and thrombin	Anti-cancer drug screening	[Siqi Du, 2015]
Gelatin/alginate/fibrinogen with HepG2[17]	$CaCl_2$ and thrombin	*In vitro* liver tumor model	[Wang et al., 2016]
Collagen/alginate/fibrinogen with pancreatic MIN6 β-cells	Thermal	Soft TE with applications in diabetic therapeutic	[Montalbano et al., 2018]
Alginate/fibrinogen/HA with Schwann cells	$CaCl_2$ and thrombin	Directing the extension of neurites (Nerve TE)	[Ning et al., 2018]
Gelatin/alginate/fibrinogen with GSC[18]	$CaCl_2$ and thrombin	*In vitro* model of GSC mechanism in tumor vascularization	[Wang et al., 2018]
Alginate/gelatin/DCEL[19]/ fibrinogen with fibroblasts and keratinocytes	$CaCl_2$ and thrombin	Skin tissue constructs	[Ramakrishnan et al., 2022]

[15] Adipose-derived stromal cells (ADSC)
[16] Polyurethane (PU)
[17] Human hepatocyte carcinoma cells (HepG2)
[18] Glioma stem cells (GSC)
[19] Diethylaminoethyl cellulose (DCEL)

2. AIM OF THE STUDY

Advances at TE have accelerated in recent years, mainly due to the contributions of 3D printing technologies and the development of more advanced materials. Various combinations of polymers have been used to create hydrogels, but each material fabrication method differs from the other and the results are sometimes not reproducible. Here, we have developed a protocol for using low viscosity materials such as 1% alginate in combination with 1% fibrinogen and demonstrated that the difficulty in producing a mechanically stable scaffold can be overcome by using the FRESH method with a gelatin support bath. In addition, the study aims to confirm that 3D printing with a mechanical extruder printer with the given settings can be used to print ADMSC, stem cells that have great potential for further studies of differentiation in artificial tissues or organs. Finally, this study aims to investigate whether 3D printing of cells is a more promising method for cell growth than culturing cells on a scaffold.

Specifically, in my master's thesis:

(1) 1% fibrinogen hydrogel with 1% alginate was prepared to increase the viscosity of the material,

(2) Scaffolds from the hydrogel were 3D printed with or without ADMSC cells using a mechanical extruder printer to study the effects of 3D printing on the cells,

(3) The materials were double cross-linked sequentially instead of simultaneously to observe whether a mechanically strong structure can be obtained that is easy to handle,

(4) The material cytotoxicity to the cells and the scaffold`s biodegradability was investigated

(5) ADMSCs were cultured on or in the scaffold for a period of 7 days to examine and compare the viability and general metabolic activity of the cells.

3. MATERIALS AND METHODS

In the following sections, the preparation of the materials used for the experiment is explained and the reason for their selection is justified. Also, the progress from the initial protocol to the final optimized protocol is explained. The Materials and Methods section is divided into four parts: (4.1) the preparation of the materials used in 3D (bio)printing, (4.2) the 3D (bio)printing process, (4.3) the culturing of the cells on and in the scaffolds, and (4.4) their characterization by various assays.

3.1 Preparation of materials used in 3D printing

3.1.1 Gelatin support bath

A fine suspension of gelatin used as a support bath for 3D printing was prepared according to the following protocol:

1. 5% gelatin suspension (w/w) was prepared with 10mM $CaCl_2$ (Honeywell, Fluka) previously cooled to 4°C. $CaCl_2$ was used as a cross-linking agent for alginate.
2. The proteins of gelatin were then hydrated by placing the gelatin suspension at 4°C for 1 hour.
3. The soaked gelatin particles were then blended at maximum speed for 1 minute using a kitchen blender (Grundig) to obtain a homogenous gelatin suspension.
4. The gelatin suspension was distributed evenly among 50-ml conical tubes (falcon tubes) and centrifuged at 800g for 5min at room temperature (RT).
5. The supernatant consisting of foam and $CaCl_2$ was removed by inverting the flasks, and gelatin granules were resuspended using fresh, 4°C $CaCl_2$ solution and centrifuged again. The process of resuspension and centrifugation was repeated until no foam was observed and a fine suspension of gelatin was obtained.
6. Since the needle used in 3D printing has a limited length, gelatin was filled into small shallow plastic containers (Figure 10).

3.1.2 Ink preparation: fibrinogen and alginate

The main material used in 3D printing was fibrinogen. However, as mentioned earlier, fibrinogen solution itself is not stable enough to form a mechanically strong and stable scaffold. Therefore, alginate was added as a material that does not affect the chemical properties of fibrinogen but contributes to the structural support of the 3D printed scaffold by cross-linking with $CaCl_2$ present in the gelatin support bath. The fibrinogen mixture with alginate was prepared according to the following protocol:

1. 4% (w/w) Alginic acid sodium salt (alginate, Sigma) was dissolved in 0.9% (w/w) NaCl (Sigma) previously prepared with deionized H_2O. To accelerate the dissolution rate, the solution was placed on the magnetic stirrer at RT for 1 hour.
2. 1.25 ml of the alginate solution was mixed after dissolution with 2.5 ml of MSC-specific Basal Medium (Human) (Stemcell Tecnologies), from now on just called medium, and 100 µl of phenol red (Sigma) for better visualization during the 3D printing process.
3. 4% (w/w) fibrinogen (Sigma) was dissolved in 1.25 ml of 0.9% (w/w) NaCl in a 5-ml syringe and incubated for 2 hours at RT until complete dissolution of fibrinogen was observed.
4. The alginate-medium solution was added to the fibrinogen solution in the syringe to a total volume of 5 ml with a final concentration of 1% (w/w) fibrinogen and 1% (w/w) alginate.
5. With the help of another empty syringe and a connector, the syringes were connected and the solution was mixed by pushing the contents from one syringe to the other several times.
6. When the contents were finally homogeneous, the solution was completely transferred into a single 5 ml syringe and was ready for 3D printing.

3.1.3 Bioink preparation: fibrinogen and alginate with cells

The bioink was prepared very similarly to the ink, except that the medium used in step 2 (see section 3.1.2) also contained 50 000 MSC cells/scaffold (50 000 cells/250µL). The culturing and preparation of the cells is described in detail in section 3.3.

3.2 3D printing

3.2.1 G-code

Geometric (G) code is a computer programming language that can be used for commanding the relative position of the nozzle with respect to the printing platform by adjusting their x, y, and z coordinates [Apro, 2008]. The G-code used in our 3D printing process was automatically generated by the Vitaprint Scaffold Generator (Figure 7), a software written for the Vitaprint 3D printer [IRNAS, 2018] used in this project (Figure 8 - left). The 3D printer used was a extrusion-based mechanical printer with 3 printing heads .

The selected settings in the program can be seen in the figure below and the final generated G-code can be found in Appendix-1.

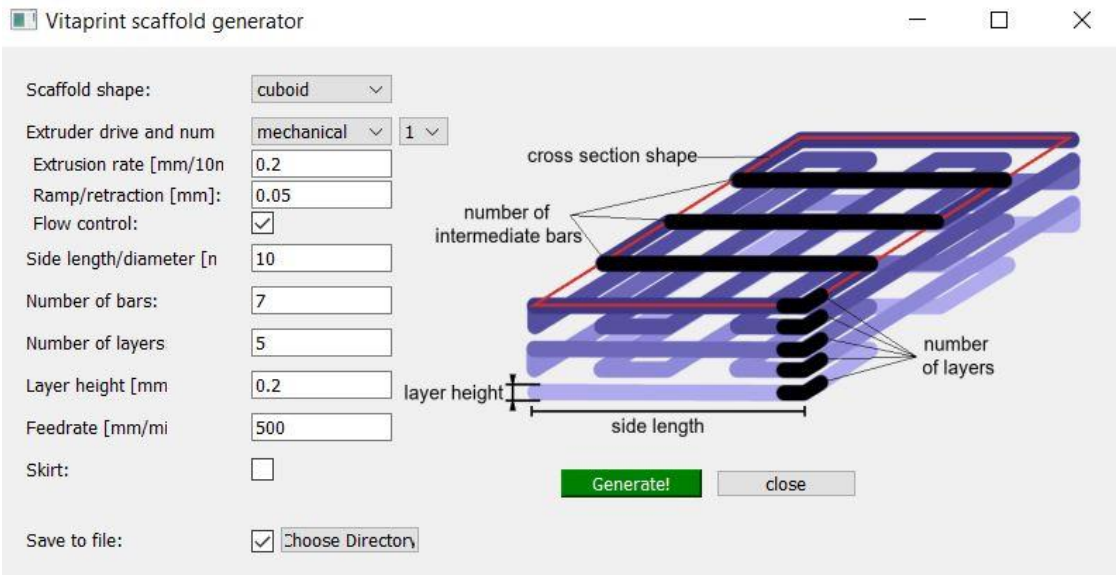

Figure 7. The set-up in the Vitaprint scaffold generator to generate G-code

The Vitaprint scaffold generator was used to create printing paths for cuboid shaped scaffolds as shown in Figure 7. The explanation of the parameters in the program is outlined in the Table below.

Tabel 5. The parameters of the Vitaprint scaffold generator and their meaning

Parameter	Meaning
Extrusion rate	The amount of material deposited from the nozzle in a unit time [Jang et al., 2021], or in our case, the amount of syringe movement during compression in z direction (in mm) per 10 mm of relative nozzle movement.
Feed rate	The speed of nozzle in plane during printing [Kaveh et al., 2015].
Ramp and retraction	The amount of material that the nozzle sucks back (in terms of a back movement of syringe in z direction in mm) during the displacement in which no material is to be deposited [Mostafaei et al., 2021].

Extrusion rate: Through a series of experiments, 0.2 mm/10 mm was determined to be the optimum extrusion rate. Since the air bubbles in the material being 3D printed are randomly distributed within the syringe, extrusion rate may need to be tailored for each experiment. For this purpose, the flow rate of the material can be manually controlled during printing by readjusting the knob on the power generator of the 3D printer (Figure 8 - right).

Feed rate: After a series of trials, the feed rate was set to 500 mm/min to obtain the optimum amount of material applied in a given moment.

Ramp or retraction: In our case, the retraction was set to 0.05 mm.

Geometry of the structure`s framework: The length of the structure was set to 10 mm, with 7 intermediate bars and 5 layers, each layer being 0.2 mm higher than the layer below. The thickness of the layer depends on the diameter of the nozzle, which in our case was a needle of 0.2 mm diameter.

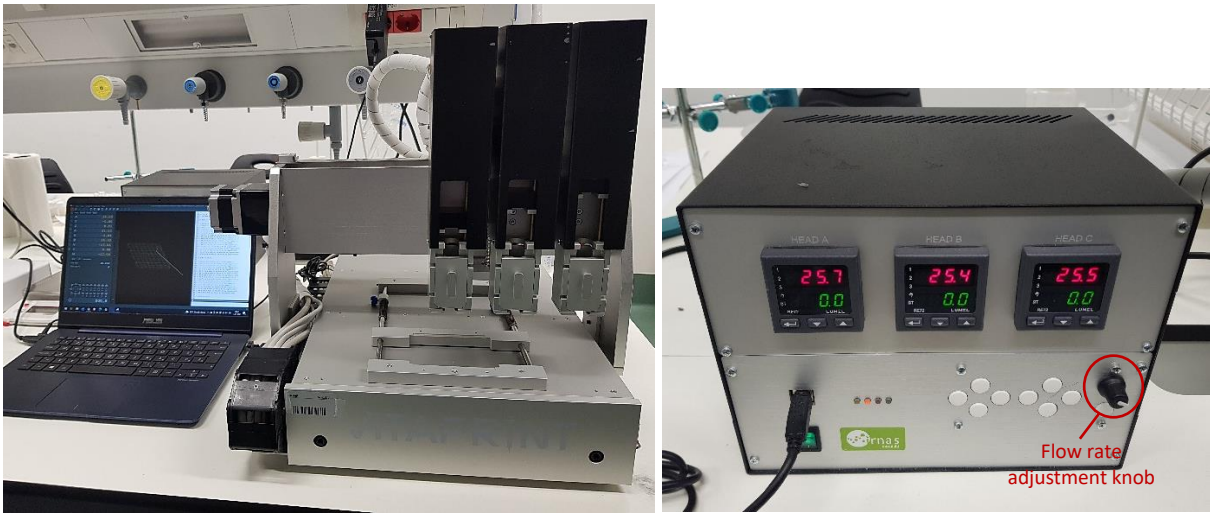

Figure 8. 3D printing device. Left: Vitaprint 3D printer connected to the computer; **Right**: the power generator with flow rate adjusting knot and temperature regulator for each printing head

3.2.2 Computer model

The computer model of the 3D scaffold (Figure 9 – middle) uses G-code as an input and is used for visualization of the nozzle path in space. The model also represents the final geometry of the scaffold to be 3D printed.

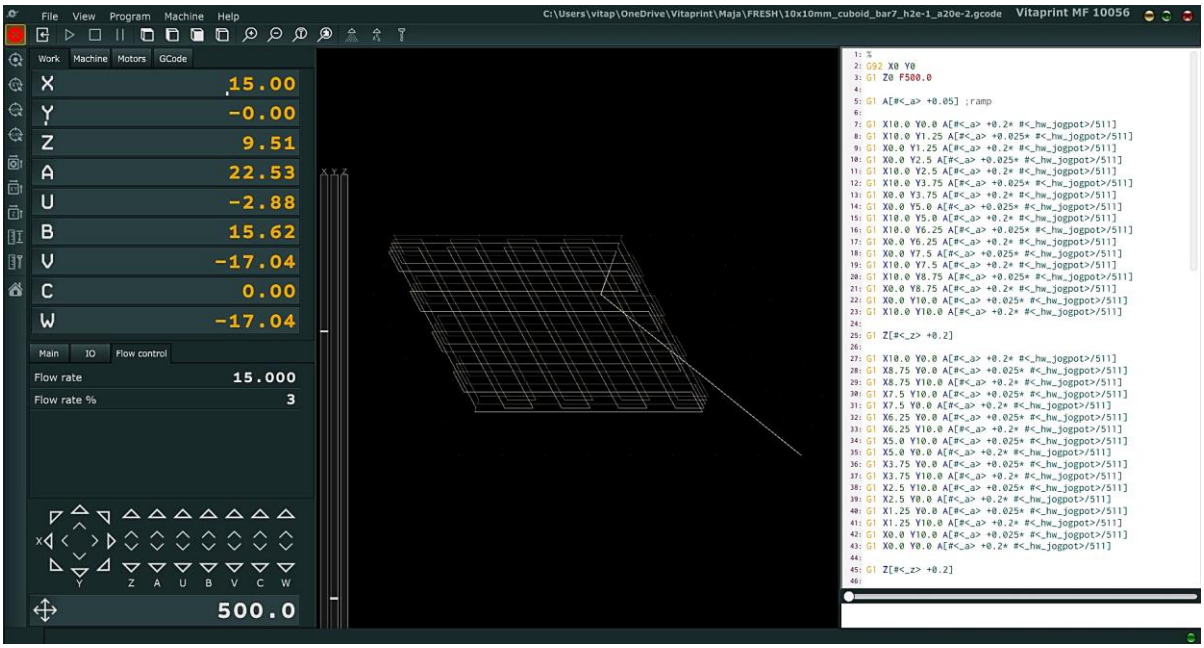

Figure 9. The outlook of the Vitaprint program. Current axes positions and command buttons on the left, computer model in the middle and the G-code on the right.

3.2.3 The 3D printing process

1. To start 3D printing, the injection with the hydrogel had to be inserted into the device (Figure 10 - left) and fixed with a small metal plate (Figure 10 - right) to prevent unwanted displacements or vibrations that could be caused by the head movement.
2. The gelatin support bath in the container was placed under the needle tip and secured with two springs (Figure 10 - left).
3. The zero position for the z-axis was determined by moving the nozzle head to the desired position, approximately 5 mm below the surface of the support bath.
4. The flow rate was set to 25 using the flow rate adjustment knob and the program was run to begin with 3D printing.
5. When a complete scaffold was produced (Figure 11), the needle was lifted to remove the container with scaffold. One scaffold was fabricated per container.
6. The scaffolds were then cut from gelatin with a scalpel and transferred to a 24-well plate. In the case of ink, this was followed by 45 minutes of UV sterilization to prevent any contamination that might have occurred during the printing process.

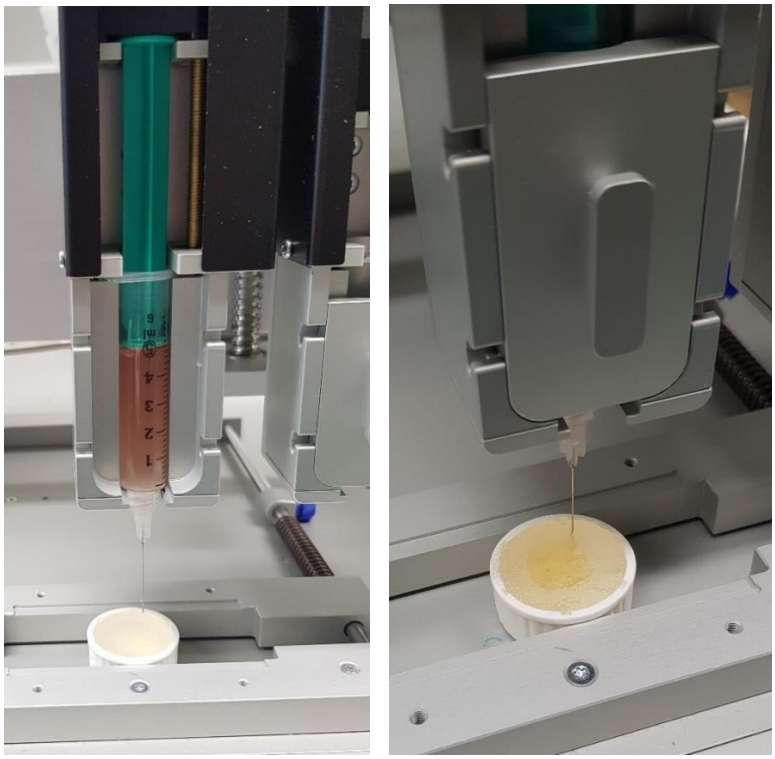

Figure 10. The 3D printing process. **Left:** The syringe with bioink inserted into the 3D printer; **Right**: The 3D printing process constructing a scaffold (in dark yellow)

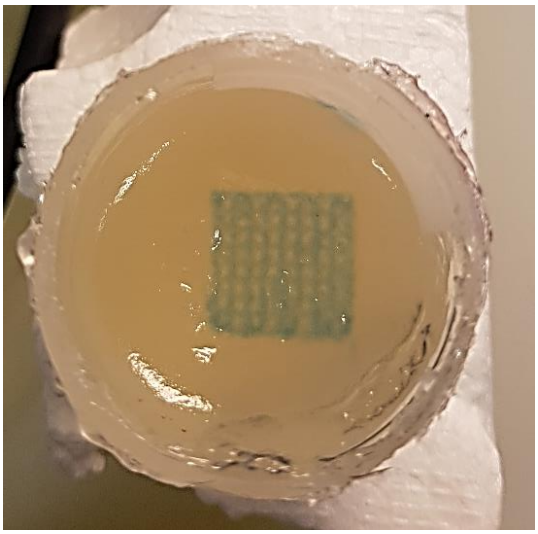

Figure 11. A top view of a scaffold printed with alginate and fibrinogen into gelatine support bath. Here, for a better representation of a web-like geometrical structure, blue colour ink was added.

3.2.4 Thrombin addition

Prior to thrombin addition, the scaffolds cut from gelatin were placed at 37°C for 1 hour to remove the excess gelatin and then transferred in fresh plates. Then, thrombin was added:

1. 1.0 U/ml of stock thrombin (Sigma) was diluted with the ADMSC-specific medium to obtain 0.1 u/ml of thrombin.
2. 70 µl of 0.1 U/ml thrombin mixed with medium was added to each scaffold and incubated at 37°C for 1 hour.
3. 1 ml of fresh medium was added to the scaffold so that the scaffold was saturated with medium and the cells added 24 hours later could not fall off.
    a. The next day, the medium was discarded from the wells to obtain as dry scaffolds as possible and 50 µl of fresh medium containing 50 000 cells was carefully added to each scaffold and to an empty well for a control.
    b. After incubation at 37°C, 5% CO_2 (later referred as incubation only) for 3 hours, 1 ml of fresh medium was added over each scaffold and incubated overnight.
4. In the case of the bioink scaffolds, thrombin was added directly to each scaffold and incubated for 1 hour. Then, 1 ml of medium was added to all wells and incubated overnight.
5. In the following days, the tests described in section 3.4 were performed on all scaffolds.

3.3 Cell culture

To avoid any contamination, all protocols involving cells (with the exception of the 3D printing process itself) were performed under a laminar flow hood.

3.3.1 Thawing and culturing the cells

1. Cells stored at -80°C were thawed rapidly by placing them in a water bath (37°C) for less than 1 minute.
2. 1 ml of the pre-warmed ADMSC-specific medium was used for diluting the cells and the cells were transferred in a 15 ml falcon tube.
3. After adding another 3 ml of medium, the tube was centrifuged at 330 rcf for 5 minutes.
4. The supernatant containing dimethyl sulfoxide (DMSO)[20] (Honeywell, Riedel-de Haen), was discarded and the pellet containing the cells was resuspended in 8 ml of medium.
5. The cell suspension was plated in a cell culture flask and incubated for 48 hours.
6. Every 48 hours, the medium in the flask was replaced with 8 ml of fresh one, until the cells were approximately 85% confluent.

[20] DMSO prevents the formation of crystals that could damage the cells during the freezing process [Verheijen et al., 2019].

3.3.2 Trypsinization of cells

In order for the cells to be used in subsequent tests and examinations, they must be detached from the surface) by the trypsinization process[21].

1. The medium was first discarded from the flask and the inner surface of the flask was washed with PBS.
2. 2 ml of trypsin was added and the flask was incubated in the incubator at 37°C and 5% CO_2 for 3-5 minutes.
3. Cells were examined under an inverted optical microscope (Axiovert 40 CFL, ZEISS) to ensure that they were completely detached from the flask.
4. 3 ml of fresh medium was then added to the flask to stop the trypsin reaction, which could damage the cells if they were exposed for prolonged time.

3.3.3 Cell counting

After harvesting, the cells were counted under the microscope to ensure that the sufficient number of cells required for the experiment had been produced.

1. 50 µL of cells were mixed in a tube with 50 µL of trypan blue stain (Sigma)[22] and pipetted into the shallow volume under the coverslip of the slide with grid for cell counting.
2. Under the microscope, the cells in the squares of the grid were counted and the corresponding equation was used to calculate the number of cells in the cell suspension per ml.
3. Depending on the number of cells needed (in our case, 50 000 cells/scaffold), the cell suspension was diluted to a certain volume by adding fresh medium.

3.4 Cell characterization

3.4.1 Cytotoxicity test (MTT assay)

One of the requirements for the material that makes up the 3D-printed scaffold is that it is not cytotoxic, or in other words, that it is biocompatible with cells [Swain and Sarkar, 2014]. This means that the material, in this case fibrin with alginate, must not have potentially harmful effects on the living cells with which it comes into contact. Performing the cytotoxicity test is especially important in the first step of the study because it tells us whether the ink should be used in the rest of the experiments and at what concentration.

Different methods can be used to test the cytotoxicity of the selected material. In this project, the MTT assay, first described by Mosmann (1983), was performed to test the cytotoxic nature

[21] Trypsin is the enzyme that degrades the proteins with which the cells adhere to the surface [Kaphalia, 2014].
[22] Trypan blue is a dye that cannot be taken up by viable cells because they have an intact membrane. Therefore, these cells have a clear cytoplasm [Strober, 2015]. In contrast, dead cells with damaged cell membranes can take up the stain and turn blue.

of our material using ADMSC. The MTT assay is a colorimetric cytotoxicity method in which a mitochondrial succinate dehydrogenase reduces yellow 3-(4,5-dimethylthiazol-2-yl)-2,5-diphenyltetrazolium bromide [Pacific Biolabs, n.d.]. The reduction produces a dark blue formazan product that is only found in living cells with fully functional mitochondria, so cell viability can be quantified.

In our MTT assay, cells were not placed directly on the scaffolds. Instead, the cells and the scaffolds were in separate plates and only the solution in which the scaffold was immersed was added over cells at different dilutions to find the concentration of materials at which the cytotoxicity of the cells was the lowest or, in other words, at which the viability of the cells was the highest.

The MTT method was performed as follows:

1. The 3D-printed scaffolds were sterilized by UV exposure for 30 minutes on each side of the scaffold.
2. The scaffolds were placed in the 12-well plate, and 1 ml of fresh medium was added. The plates were incubated for 24 hours.
3. ADMSC cells were then harvested and counted as previously described. The experiment was performed in 4 replicates and at 4 different dilutions (1:1, 1:2, 1:4, and 1:8), with a control added at each replicate. 10 000 cells were used per well.
4. 100 µL of the cell suspension was added to 40 wells of a 96-well plate and the cells were incubated for another 24 hours.
5. The next day, the medium was removed from all cell wells by inverting the plate.
6. Fresh medium was added to each well containing cells at the following dilutions:
    - Control (100 µL fresh medium only)
    - 1:1 (100 µL fresh medium + 100 µL scaffold medium)
    - 1:2 (100 µL fresh medium + 100 µL medium from the 1:1 dilution well)
    - 1:4 (100 µL fresh medium + 100 µL medium from the 1:2 dilution well)
    - 1:8 (100 µL of fresh medium + 100 µL of medium from the 1:4 dilution well)
7. 100 µL of medium from the last 1:8 dilution well was discarded to obtain the same volume of 100 µL in all wells.
8. The plate was then incubated for 24 hours.
9. 100 µL of the 10% MTT solution prepared from MTT reagent (Sigma) and fresh medium was added to each well on the next day and the plate was incubated for 3 hours.
10. The MTT solution was then removed from all wells using a suction pump. This step had to be done carefully to preserve the crystals formed by the MTT reagent.
11. 100 µL of DMSO was added to each well to dissolve the crystals. At this time, the formation of a purple color could be observed.
12. The plate was shaken for 10 minutes or until a homogeneous solution without dark crystal spots was observed.
13. Finally, the absorbance was measured with the spectrophotometer at 570 nm.

3.4.2 Degradation test

The rate of degradation depends not only on the rate at which the chemical bonds between the polymer chains that make up the scaffold are broken, but also on the geometry and architectural network determined by the 3D printing process [Madl et al., 2018]. The strength of the chemical bonds depends on the cross-linking process, which in our case was ionic and enzymatic. The ionic bonds were formed between the calcium ions and the alginate polymer chains [Indurkar et al., 2020] and the enzymatic reaction occurred between fibrinogen and thrombin to form fibrin. The rate of degradation of a hydrogel should ideally match the rate at which cells can build their own ECM [Saroia et al., 2018].

The degradation assay was performed as follows:

1. Scaffolds were 3D printed according to the geometry set with the parameters from Figure 7 and then placed in 24-well plates.
2. The plates were stored at -80°C for 3 hours and then freeze-dried overnight to dry.
3. The scaffolds were then weighed and returned to the well plate, where 1 ml of sterile PBS was placed over each scaffold.
4. Weighing was performed at 24, 48, 72 hours, 5 days, 7 days, and 2 weeks. After the first 24-hour period, the first scaffolds were removed from the PBS, transferred to a fresh corrugated plate, and stored at -80°C.
5. The same procedure was followed for the remaining time points until the scaffolds were deemed too unstable for further measurements.
6. All scaffolds from -80°C were freeze-dried overnight and weighed the next day.

3.4.3 Live/Dead assay

Performing a live/dead test allows us to distinguish viable from dead cells and determine the viability of the cells on the 3D-printed construct [Thermo Fisher, n.d.]. In addition, the test is useful for investigating the success of cell attachment to the bioink. The live/dead assay uses a combination of a calcein-containing dye that fluoresces green upon interaction with the esterase enzyme of live cells and their intact cell membrane, and ethidium homodimer that binds the DNA of dead cells with damaged cell membranes and produces red fluorescence.

The Live/Dead assay was performed for both cases, when the cells were on and in the scaffold:

1. The medium was completely removed from all wells containing scaffolds as well as from the control containing cells grown directly in a plastic well.
2. 10 ml of the medium was mixed with 5 µL calcein (Invitrogen) and 20 µL ethidium homodimer (Invitrogen) to make a live/dead mix.
3. 1 ml of the mixture was then added to each well and incubated for 45 minutes.
4. After incubation, the scaffolds were removed from the wells and placed upside down on the slide to be observed under the EVOS FLoid Imaging System microscope (Thermo Fisher) at various magnifications. Cells in the wells were observed directly from the plate after the live/dead mix was discarded.

3.4.4 Alamar Blue assay

Once it is clear that the material itself is not cytotoxic and that the printing process also does not damage the cells, further cell analysis can be performed. In MTT assay, the cytotoxicity of the material to the cells was observed, providing us with the information on cell viability only, but not on the actual metabolic activity of the cells that accounts for their proliferation and how it changes over time under different experimental conditions (cells growing *in* versus *on* the scaffolds). To detect the metabolic activity and quantitatively measure it, Alamar Blue staining [Thermo Fisher, n.d.] can be performed. The reagent in Alamar Blue assay contains resazurin, a nontoxic substance that is reduced by the live cells to resorufin, which produces red fluorescence and can be detected spectrophotometrically.

The Alamar Blue assay was performed as follows:

1. The medium was completely removed from all wells.
2. The scaffold were transferred into fresh 24-well plate.
3. Alamar Blue reagent (Sigma) was diluted 1:240 with fresh medium.
4. 2 ml of the reagent was then added to each well (Appendix 2) and the plate was shaken for 30 seconds and incubated for 3 hours.
5. After incubation, 100 µl of reagent from each well was transferred to a 96-well plate in triplicate and the plate was shaken for 5 minutes.
6. The fluorescence was measured at 530 nm excitation wavelength and 590 nm emission wavelength using the Varioskan Flash Spectrophotometer (Thermo Scientific, USA).

3.4.5 Nano-CT imaging

Nano-computed tomography (nano-CT) is a high-resolution 3D imaging technique that can help us understand the internal structure of an object such as a 3D-printed scaffold [Kampschulte et al., 2015]. The technique uses X-rays and an electronic detector array to create patterns of varying densities that are combined to form a 3D image. As the object rotates on the platform, multiple X-rays penetrate the object to capture the 3D cross-sectional view with nanoscale detail [zeiss.com, n.d.].

In this project, ZEISS Xradia 620 Versa (Carl Zeiss AG, Oberkochen, Germany) nano-CT device was used to assess the internal structure of bioink scaffold and compare it to the control scaffold:

1. The freshly 3D printed scaffolds were cross-linked as described earlier.
2. The scaffolds were frozen at -80°C and lyophilized (freeze-dried).
3. The dry scaffold was placed between two holders on the platform and the measurements were done at 4x magnification at 30kV and 2W, without an additional filter. Exposure time was set to 1 second and binning was set to 2.
4. The generated image was reconstructed and analyzed using ZEISS Xradia software and NIH image analysis software (NIH, MD, USA) respectively.

3.5 Statistical analysis

The statistical significance of cytotoxicity results (MTT test) was determined by a one-way ANOVA test study and the statistical significance in Alamar Blue test was determined by Two-way ANOVA test study, with all the details in the Results section.

Normal distribution was determined by Shapiro-Wilk test. P-values were presented as statistically significant at 95% level of confidence as $P < 0.05$, where $P < 0.05$ is for significantly different from the rest of the groups.

4. RESULTS

4.1 Cytotoxicity test with MTT

As shown in Figure 12, 1:1, 1:2, and 1:4 dilutions resulted in higher cell viability than the control, with the 1:1 dilution having a viability of 1.09 compared to the control, the 1:2 dilution having a viability of 1.22, and the 1:4 dilution having a viability of 1.11. At a dilution of 1:8, using 1 unit of medium from the scaffolds and 8 units of fresh medium, the viability was 0.14 lower than the control.

The Shapiro-Wilk tests did not show a significance departure from the normality, $p > 0.05$, and it is assumed that the data is normally distributed. The p-value of the One-way ANOVA test is ≤ 0.001, indicating that the difference between the dilution ratios is statistically different.

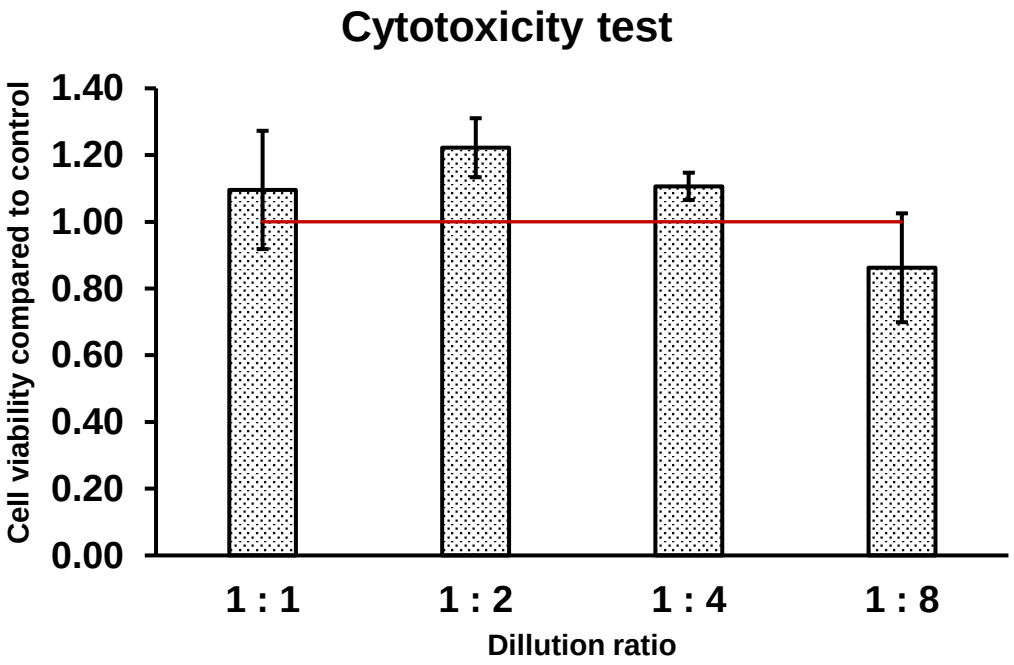

Figure 12. The cytotoxicity test with MTT reagent. The average value of 4 replicates was considered. The control consists only of cells in fresh medium and is shown as a red line with the value of 1, meaning 100% cell viability. The dilutions on the x-axis represent the ratio of fresh medium to scaffold medium, the y-axis shows the viability of the cells compared to the control and the error bars represent the standard deviation. Differences between dilution ratios: *** $p \leq 0.01$ were calculated using ANOVA.

4.2 Degradation test

The results of the degradation test show that the weight of the scaffolds decreased over a seven-day period (Figure 13). With an initial weight of 100%, the weight decreased by almost 10% in the first 24 hours. After 48 hours, on average 78% of the weight was still present, and after 3 days the weight of the scaffold dropped to 73%. The next measurement was taken on 5^{th} day after the first incubation in PBS. It was observed that the weight dropped to 58% of the original value. 2 days later, only slightly more than 50% of the scaffold was still present, while the rest had degraded. The remaining scaffolds were too unstable to reliably continue measurements. Therefore, only a total degradation time of 7 days was considered.

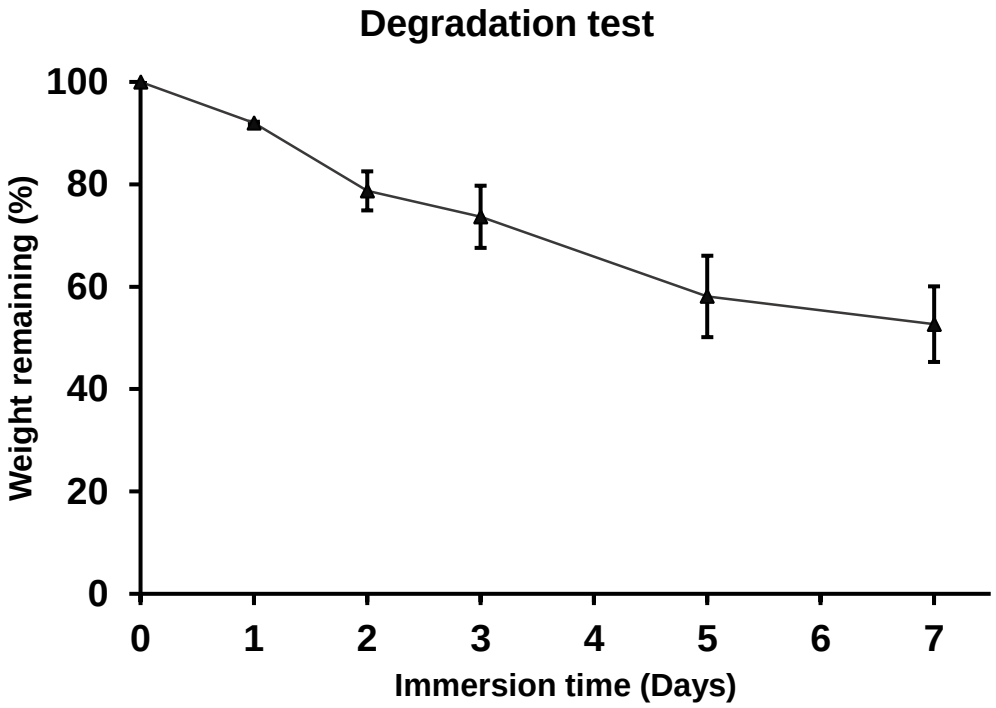

Figure 13. Degradation test. The test was performed on scaffolds without cells. X-axis represents the immersion time and y-axis represents the average remaining weight (in %) from the initial 100%, measured on the given days. The error bars represent the standard deviation.

4.3 Cell viability test with Live/Dead assay

Figure 14 shows images from the microscope under 4x magnification with live and dead cells stained with calcein (green) and ethidium homodimer (red), respectively. Most growth is seen after 7 days in the control sample (cells cultured without contact with the scaffold) and less in the ink (cells on the scaffold) and bioink (cells in the scaffold) scaffolds. In addition, morphological changes in cell shape from circular to more elongated can be observed over time in the control case. Overall, cells in the control well remained evenly distributed and viable for 7 days.

In the test experiment where the cells were placed on the scaffold, very few dead cells were observed on day 7. However, in this case, the cells were not as evenly distributed as in the control. Instead, the cells appeared to be clustered on the scaffold. It can be observed that the number of cells on the scaffold decreased over the course of 7 days, although no red dots representing dead cells could be seen. It should be mentioned that when checking the well in which the cells were incubated on the scaffold, most of the cells were found at the bottom of the well, indicating that they were not able to attach to the material when they were placed on the scaffold.

In the final test, when the cells were 3D printed with the material as bioink, it was seen that the cells were evenly distributed across the scaffold, but with a lower cell density than the control. Although the morphology of the cells was not as clear as the control, which was due to the fact that they were encapsulated in the scaffold, the number of cells appeared to increase over 7 days. In addition, no dead cells were observed under the microscope, and no cells were found at the bottom of the well in which the bioink scaffold was incubated.

When comparing the ink and bioink scaffolds, it is clear that the bioink scaffold exhibited higher cell proliferation and a more even distribution of cells than the scaffold to which the cells were applied after the 3D printing process. While proliferation of cells encapsulated in the scaffold increased over a 7-day period in the case of the bioink, it decreased in the case of cells placed on the scaffold.

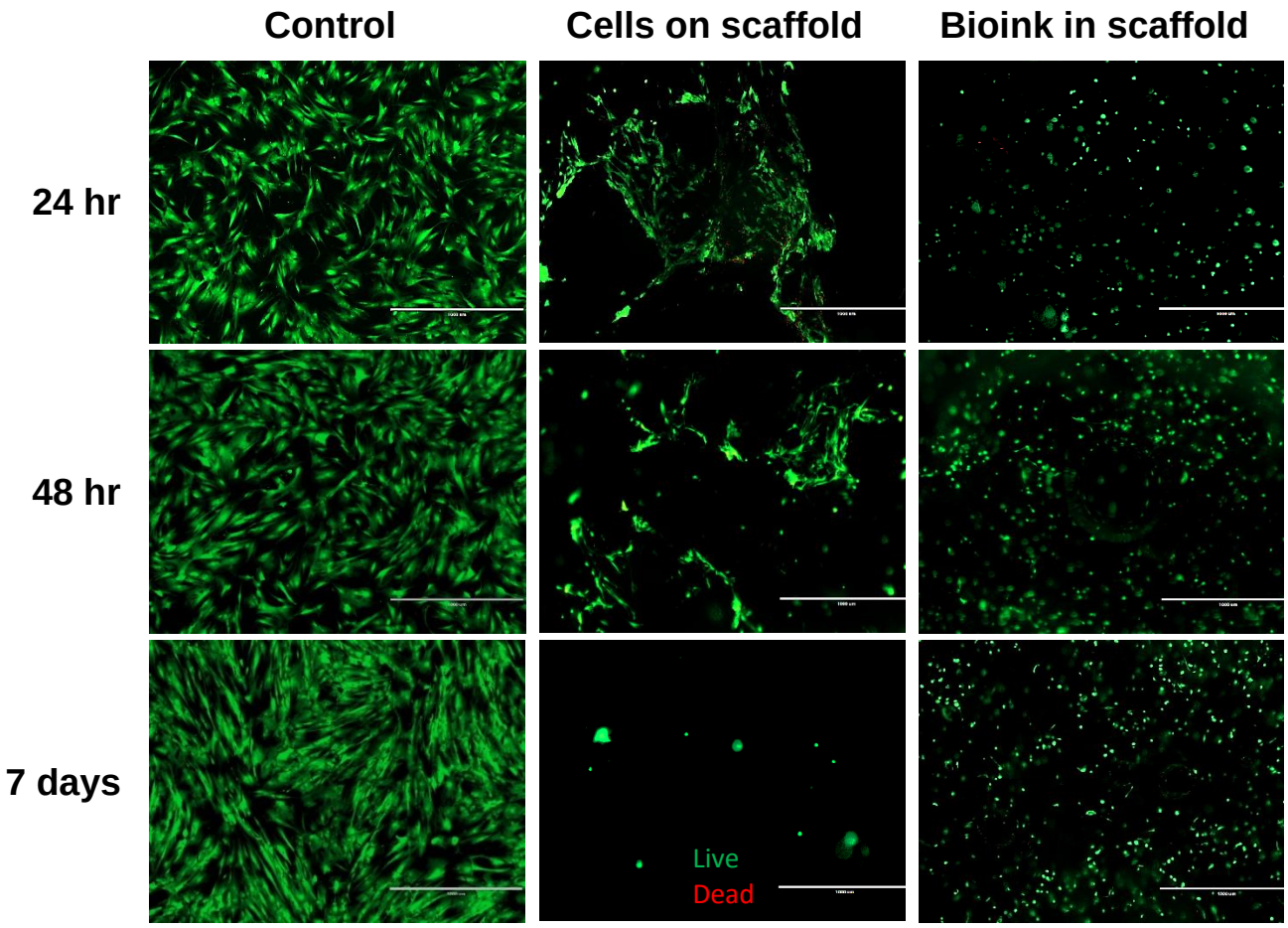

Figure 14. Live/dead assay. The assay was performed 24 hr, 48 hr and 7 days after incubation of cells either on scaffolds or as bioink in scaffolds to assess cell viability. Green colour represents live cells and red colour represents dead cells. Magnification: 4x

4.4 Overall cell metabolic activity test with Alamar Blue assay

The results of the Alamar Blue assay in Figure 15 show that the control had the highest total cell metabolic activity at all time points, confirming active cell growth. Metabolic activity increased over the course of 7 days, reaching 773 emitted fluorescence on day 7. The opposite trend was observed for cells placed on the scaffold. In this assay, metabolic activity was already lower than in the control after the first 24 hours with a fluorescence of 187. A decrease is observed over the next few days, with the lowest metabolic activity reached on day 7.

In the case of the bioink scaffold, the cells were less metabolically active (111 emitted fluorescence) in the first 24 hours than in the case of the cells on the scaffold (24 hours). However, metabolic activity increased subsequently, reaching a fluorescence of 213 after 48 hours and an even higher fluorescence of 329 on day 7. Overall, the cells in the control showed the highest metabolic activity. Comparison of the two experiments shows that the bioink scaffold resulted in higher overall metabolic activity of the cells than the scaffold to which the cells were applied after the scaffold was already 3D printed.

The Shapiro-Wilk test revealed a normal distribution ($p > 0.05$) for all time points. Similarly, no significant difference from the normal distribution ($p > 0.05$) was found for any of the scaffold types. Therefore, it is assumed that the data are normally distributed and the ANOVA test can be applied.

The p-value of the two-way ANOVA for the variable "time" is > 0.05. Therefore, it is assumed that the difference between the time points 24 hours, 48 hours and 7 days is not statistically different.

On the other hand, the p-value of the two-way test ANOVA for the variable "scaffold type" is ≤ 0.05. Therefore, it is assumed that the difference between the control, the cells on the scaffold and the bioink scaffold is statistically different..

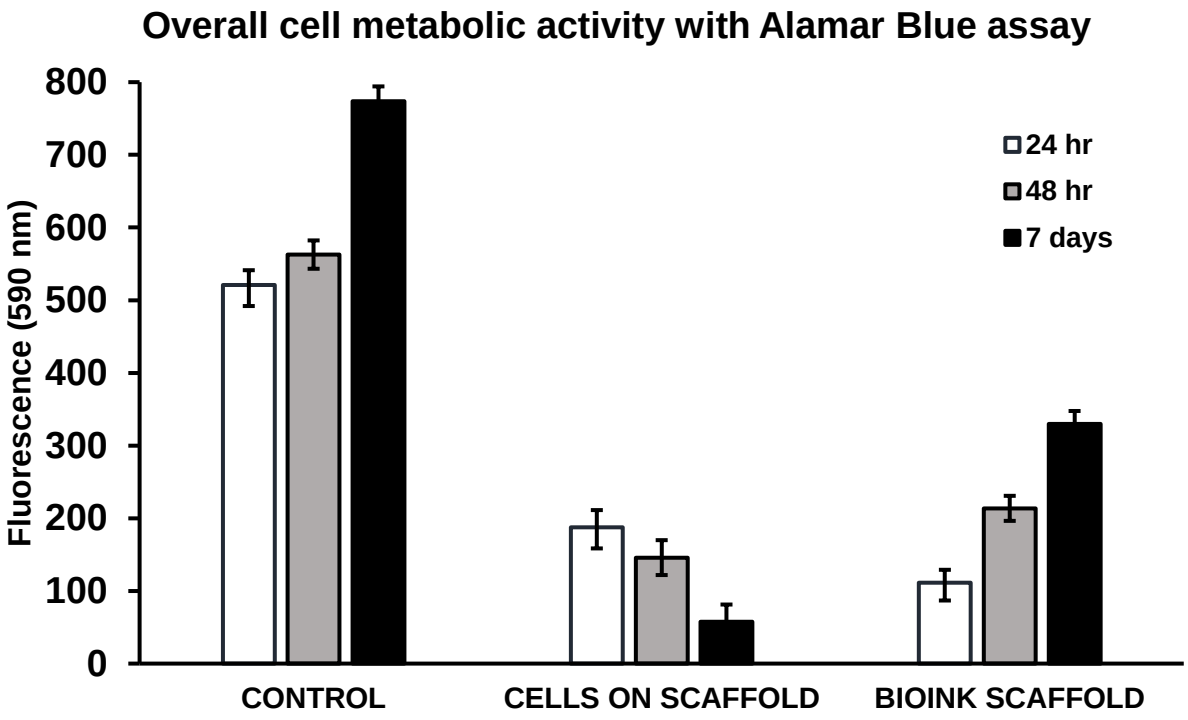

Figure 15. Alamar Blue assay for total cell metabolic activity. The white columns represent the first 24-hour period, the grey columns represent the 48-hour time point, and the black columns represent the 7th day after the first incubation. The Y-axis represents the intensity of the emitted fluorescence at 590 nm and the error bars represent the standard deviation.

4.5 Nano CT imaging

Figure 16 clearly shows the fibrin hair-like structure that makes up the scaffold. The hairs are interconnected and provide an extensive ECM environment for cell attachment and growth. In Figure 16-left, holes can be seen that were created during the 3D printing process. This indicates that the desired geometry of the mesh-like structure could be achieved. In Figure 16-right, white dots can be seen, which could be cells encapsulated in the scaffold structure. However, further investigation should be performed to confirm that the white dots do indeed represent the ADMSC, but this was out of the scope of this thesis.

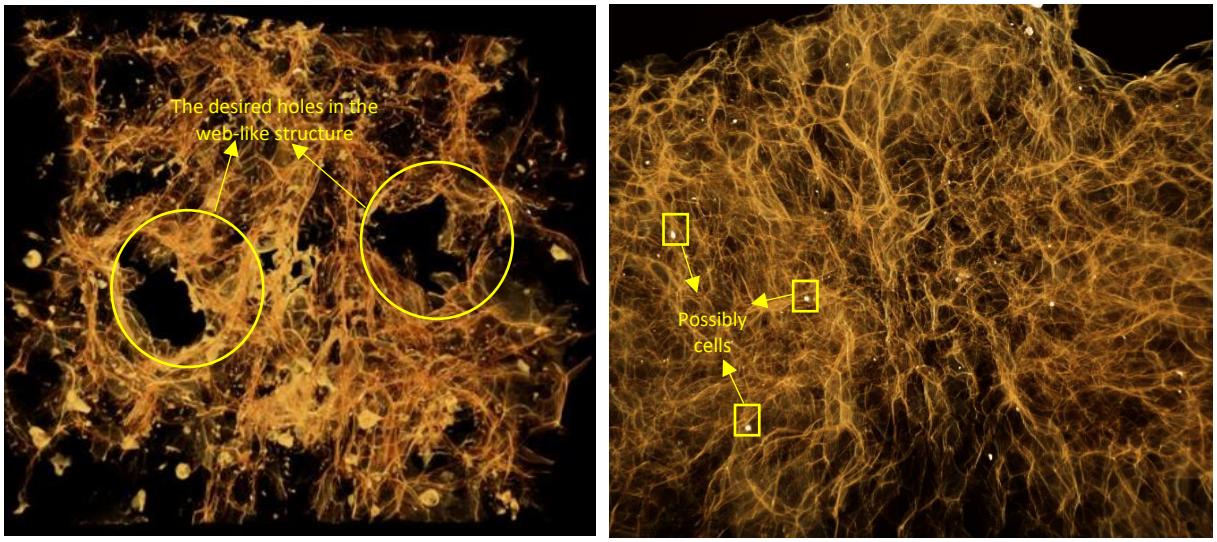

Figure 16. Nano-CT images of scaffold without cells or control (left) and bioink scaffold (right) at 4x magnification. For better presentation orange colour filter was used.

5. DISCUSSION

In this study, a protocol for the preparation of low viscosity materials was developed and used for 3D printing of ink and bioink from alginate and fibrinogen scaffolds. ADMSCs were used with the given hydrogel formulation and biocompatibility and viability experiments were performed.

Hydrogels have been shown to be ideal networks for cell attachment and interaction in TE and serve as an artificial ECM platform for cell growth and proliferation. In this project, a hydrogel was prepared from fibrin and alginate. Fibrin and alginate were chosen as natural polymers because they both have advantageous properties for optimal scaffold formation, as shown in Figure 6.

Several studies have used 3D bioprinting technologies to fabricate scaffolds from alginate and fibrinogen and have been summarized in Table 4. However, most of these studies used a high concentration of alginate or another highly viscous material such as gelatin to overcome the problem of low mechanical stability and directly 3D print a strong and stable scaffold [see Table 4]. Unfortunately, alginate has not been shown to have as desirable effects on cell growth as fibrinogen [Nakamura et al., 2010]. On the other hand, alginate provides excellent mechanical stability, which is critical when constructing a scaffold.

Since fibrinogen alone has too low viscosity, the lowest possible concentration of alginate (1%) was used in this master's thesis. The hydrogel produced was still too unstable to directly 3D print a structure capable of maintaining its shape in a given geometry. Therefore, a FRESH method was used with a gelatin support bath to demonstrate that lower viscosity materials can be 3D printed without adding a significant concentration of another, more viscous material, but still sufficient to initiate the cross-linking process.

Alginate cross-linked with $CaCl_2$ in the gelatin support bath and formed strong bonds that allowed us to print architecturally well-defined structures in multiple layers. The $CaCl_2$ concentration was low enough to allow rapid gelation while stabilizing the extruded material and allowing the new layer of material to bond to the layer below.

Normally, $CaCl_2$ is added after printing and reacts immediately with the alginate. In our case, however, this was not possible because too low a concentration of alginate was used, which did not allow us to print without a support bath. Therefore, $CaCl_2$ had to be added directly to the support bath so that the alginate came into contact with it as soon as the hydrogel was extruded from the syringe. Once a bond was established between the alginate and $CaCl_2$, an ECM-like structure started to form, allowing the cells to attach, migrate, communicate, and proliferate.

For this project, it was important to make a support bath with a very fine gelatin suspension that would allow 3D printing of a construct at high resolution. If the suspension was not fine enough, the 3D printing process could have been disrupted by the needle getting stuck

between large particles, resulting in uneven material deposition and lower resolution. Using the protocol described in the Materials and Methods section, a needle could easily move through the support bath and continuously deposit a material to create the desired geometry. Thanks to the mechanical properties of gelatin and alginate, the final scaffold structure was very well supported and maintained its shape, as shown in Figure 11.

A second cross-linking occurred when fibrinogen was polymerized by thrombin, further strengthening the structure. The use of only 1% cross-linked alginate in previous experiments did not result in a stable scaffold that could be easily handled [Wang et al., 2021]. To reduce the amount of thrombin required, which is very expensive, the enzyme was added to the scaffold after it was removed from the support bath. In this way, thrombin could be more concentrated and act more efficiently on the fibrinogen without being unnecessarily diluted by the additional gelatin in the support bath. It was possible to remove a single cross-linked scaffold from the support bath prior to the application of thrombin, as it was still entrapped in the support bath, since alginate also forms bonds with gelatin. Only after incubation at 37°C did the gelatin melt and only the scaffold, which was also double cross-linked with thrombin, remained. After complete polymerization, a very stable scaffold with the desired geometry was obtained, which was easy to handle and could be used for cell characterization.

MSCs were selected for this project because they have previously been shown to respond very positively to fibrin. This was determined by a cytotoxicity or biocompatibility assay using the MTT reagent. As can be seen in Figure 12, cell viability was found to be greater than 80% at all dilution ratios, which is sufficient to confirm that the 1% alginate and 1% fibrinogen scaffold does not produce a cytotoxic substance that would decrease cell viability [ISO, 2009]. The highest cell viability compared with the control was observed at a dilution of 1:2, suggesting that to achieve the optimal concentration of alginate and fibrin in a scaffold, the current concentrations should be reduced by half.

After making sure that the material itself was not cytotoxic, the cells were 3D printed as bioink. As can be seen from the live/dead test results in Figure 14, no dead cells were observed. This indicates that the shear stress caused by the movement of the cells through the needle into the gelatin at the given parameters for velocity and flow rate is not harmful to the cells and can be used as a reliable method to produce scaffolds from bioink.

Not only was the bioink scaffold fabricated, but also scaffolds of only alginate and fibrinogen (ink) were 3D printed and the cells were applied to them. Since the top surface of the ink scaffold was not perfectly uniform (the ink was deposited as a bar with some empty spaces in between), a problem occurred when the cells were applied to the top of the scaffold. Namely, the cells could not settle on an uneven, wet surface and slid down, resulting in a buildup of cells at the bottom of the well instead of on top of the scaffold. To prevent this, medium without cells was first added to the scaffolds to allow them to become completely saturated with liquid. The next day, the medium was completely removed, left to dry for a while, and then the cells were very carefully placed on the scaffold in a very small volume of medium.

The medium is required by the cells for survival. Therefore, the cells were left in a small volume of medium for only 3 hours and then covered with additional medium. It is very likely that many cells were not able to attach to the scaffold in this short time, causing the cells to slide off the scaffold. This is also evident from the live/dead sample results (Figure 14) and confirmed by the Alamar Blue assay (Figure 15). In Figure 14, the number of cells on the scaffold is much lower compared to the control and actually decreases over time. A similar decrease in cell viability can be seen in the Alamar Blue results in Figure 15.

It is possible that some cells died during the 7-day period, causing them to lose attachment and slip off the scaffold. As a result, these cells are not visible in Figure 14, because the scaffold was transferred into fresh well plate prior to addition of Alamar Blue reagent. Another possible reason could be that the scaffold fell apart after some time and the connections between the cells and the surface of the scaffold broke. Furthermore, since the old medium was removed before the fresh medium was added, the weakly adherent cells were removed from the plate.

Comparing the cells on the scaffold to the cells in the scaffold, the results suggest that bioink is a much more efficient method of bringing cells into contact with the scaffold. When the cells were printed with the material, they encapsulated in the fibrin network with hair-like structure, as shown in Figure 16. The fibrin network, which was further supported by cross-linked alginate, allowed the cells to grow and proliferate without being washed off with fresh medium. In addition, the survival rate of the cells was higher in the bioink because the cells were continuously present in a sufficient volume of medium, in contrast to the cells that were placed on the scaffold and attempted to survive in a minimal volume of medium for 3 hours.

Similarly, the live/dead results show that the viability of the cells was higher in the bioink than in the ink. It can be clearly seen that the cells in the bioink were able to proliferate successfully and attach firmly to the alginate-fibrin matrix over time. In addition, the cells in the bioink were evenly distributed across the scaffold, in contrast to the clusters of cells observed on the ink scaffold. Although the cells in the control case appeared to have much better morphology and began to interact with each other, it should be noted that the control cells were grown in a 2D culture, which was not as representative as a 3D culture in a bioink scaffold. In addition, the cells inside the scaffold were encapsulated in an extensive network, which was likely the reason they looked roundish rather than elongated like the control cells. It is expected that over time, the cells in the scaffold will have a similar longitudinal morphology and begin to interact with each other.

The results from Alamar Blue support the observation that the cells in the scaffolds had higher metabolic activity than the cells on the scaffolds. The graph in Figure 15 shows that in the first 24 hours after the initial incubation with cells, the metabolic activity was higher in the cells on the scaffolds than in the bioink scaffolds. A possible explanation for this could be the stress to which the cells were exposed during the 3D printing process. Indeed, the shear stress to which the cells were subjected when they were placed in the support bath may have delayed their

development, resulting in initially (in the first 24 hours) lower metabolic activity. However, over time, the metabolic activity of the cells in the bioink became higher than that of the cells on the scaffolds. The difference became even greater after 7 days. These results suggest that the bioink is a more suitable network for successful cell proliferation than when the cells are attached to the scaffolds after 3D printing is completed.

As mentioned in the introduction, an optimal scaffold is biodegradable and allows cells to build their own ECM in the space that was previously scaffold. The rate of degradation should ideally match the rate of formation of new ECM, as mentioned earlier. The formation of new ECM can be measured by detecting collagen [Finamore et al., 2019], a structural protein produced by cells during ECM assembly, but this was beyond the scope of this project. A rate of degradation that is too fast or too slow could be detrimental to the tissue [Yannas, 2001]. From the results in Figure 13, 50% of the scaffold was degraded in only one week. Such a degradation rate could be considered too fast, as it does not allow enough time for the cells to build their own ECM and provide for their own mechanical support. To slow down the degradation rate, the concentration of cross-linking agents, namely $CaCl_2$ and thrombin, could be increased, creating stronger bonds between the monomers and chains of the hydrogel.

Overall, this master's thesis provided a protocol for 3D printing low viscosity materials into a support bath, either with or without cells, and the 3D printing process did not harm the cells. In addition, the given material formulation was non-cytotoxic, biodegradable, and stimulated cell proliferation, providing a great foundation for future cell differentiation studies with various applications in regenerative medicine.

6. CONCLUSIONS and PERSPECTIVES

TE has been transforming the field of regenerative medicine for several decades. Progress has accelerated since the development of 3D printing technologies, adding another dimension to the TE field, enabling the production of *in vitro* tissue models with sophisticated geometries for use in drug testing, disease modeling, and artificial organ transplantation.

In this study, a geometrically defined and mechanically stable structure was 3D printed from a hydrogel composed of two natural polymers, 1% alginate and 1% fibrin, in a gelatin support bath. Without the support bath, 3D printing of hydrogels with such low viscosity would not be possible, making FRESH an efficient method with good prospects for future studies with low viscosity materials such as fibrinogen, which has been shown to have very beneficial effects on cells.

In addition, the study used dual cross-linking, which unlike some other studies was not performed simultaneously. This study confirms that cross-linking of alginate with $CaCl_2$ is immediate and sufficient to initially maintain the structure until the second cross-linking of fibrinogen with thrombin occurs a few hours later to create bonds for further strengthening of the scaffold. This approach allowed thrombin to be used in a smaller volume, making it more economical as the scaffold was removed from the gelatin bath and the excess gelatin melted away before thrombin was added. Also, since alginate forms bonds with gelatin, it would be more difficult to remove the scaffold if it remained in the support bath while allowing a slow enzymatic reaction between fibrinogen and thrombin.

This study also confirmed that the two polymers provided a promising platform for cell growth, especially for ADMSC cells, which used them efficiently for their growth and proliferation. Each hydrogel material contributed its properties to the scaffold fabrication, with alginate providing mechanical strength and fibrinogen providing successful cell attachment and proliferation. The results of this work suggest that both materials are not only biocompatible with ADMSC but also stimulate their proliferation, giving fibrinogen in particular great potential for future cell differentiation studies. In addition, the cells responded positively to the growth conditions, suggesting that neither thrombin nor fibrinogen could be cytotoxic to this cell type. Furthermore, it can be said that the rate of degradation as observed in this project, with some modifications to the protocol, such as increase in the concentration of cross-linking agents, makes alginate and fibrin scaffolds very good candidates for use in tissue repair and artificial organ transplantation.

In addition, further studies should be performed on the Nano- CT device to investigate whether the white dots on the image are actually the cells or a cross-linking agent used in the experiment. Nano- CT provides great insight into the spatial arrangement of (possibly) cells and has great potential to study the effects of different material concentrations and scaffold geometries on cell distribution within the scaffold. Finally, the goal of the study was to find optimal 3D printing conditions to avoid damaging the cells in the bioink and to print a

mechanically stable scaffold. The study successfully showed that 3D printing did not damage the cells with the given printing settings. Although the growth of the cells was initially hindered, the metabolic activity increased over the next few days and exceeded the activity of cells cultured on a scaffold. This confirms that using cells with hydrogels in 3D printing is a more efficient method than culturing cells in a 2D culture or making molds and using them as a platform for cell growth, as suggested in some other studies in introduction. In addition, the bioink scaffold provides a 3D environment similar to that of native tissue, which offers great potential for future studies on *in vitro* tissue or organ models and drug testing.

Overall, it can be concluded that 3D bioprinting is an efficient method for creating an architecturally desirable structure that allows cells to be metabolically active through nutrient exchange, waste removal and access to oxygen. This is not as efficient or representative when culturing cells in a simple 2D cell culture on a Petri dish or placing them on a scaffold.

The ultimate goal of this study, to develop an efficient method for 3D printing low viscosity hydrogels with cells and to demonstrate that cells can successfully grow and proliferate in scaffolds, was achieved. The study lays the foundation for future advances in TE using fibrinogen as the main component of hydrogels for scaffold fabrication..

REFERENCES

Abdallah, B. M., & Kassem, M. (2008). Human mesenchymal stem cells: from basic biology to clinical applications. Gene Therapy, 15(2), 109-116. doi:10.1038/sj.gt.3303067

Abelseth, E., Abelseth, L., De la Vega, L., Beyer, S. T., Wadsworth, S. J., & Willerth, S. M. (2019). 3D Printing of Neural Tissues Derived from Human Induced Pluripotent Stem Cells Using a Fibrin-Based Bioink. ACS Biomaterials Science & Engineering, 5(1), 234-243. doi:10.1021/acsbiomaterials.8b01235

Afewerki, S., Sheikhi, A., Kannan, S., Ahadian, S., & Khademhosseini, A. (2018). Gelatin-polysaccharide composite scaffolds for 3D cell culture and tissue engineering: Towards natural therapeutics. Bioengineering & translational medicine, 4(1), 96-115. doi:10.1002/btm2.10124

Afghah, F., Altunbek, M., Dikyol, C., & Koc, B. (2020). Preparation and characterization of nanoclay-hydrogel composite support-bath for bioprinting of complex structures. Scientific Reports, 10(1), 5257. doi:10.1038/s41598-020-61606-x

AlamarBlue™ cell viability reagent. Thermo Fisher Scientific - US. (n.d.). Retrieved April 15, 2022, from https://www.thermofisher.com/order/catalog/product/DAL1025

Aliborzi, G., Vahdati, A., Mehrabani, D., Hosseini, S. E., & Tamadon, A. (2016). Isolation, Characterization and Growth Kinetic Comparison of Bone Marrow and Adipose Tissue Mesenchymal Stem Cells of Guinea Pig. International Journal of Stem Cells, 9(1), 115–123. doi:10.15283/ijsc.2016.9.1.115

Alihosseini, F. (2016). Plant-based compounds for antimicrobial textiles. Antimicrobial Textiles, 155–195. doi:10.1016/b978-0-08-100576-7.00010-9

Angra, V., Sehgal, R., Kaur, M., & Gupta, R. (2021). Commercialization of bionanocomposites. Bionanocomposites in Tissue Engineering and Regenerative Medicine, 587–610. doi:10.1016/b978-0-12-821280-6.00017-9

Apro, K. (2008). Secrets of 5-axis machining. Industrial Press.

Atala, A., Bauer, S. B., Soker, S., Yoo, J. J., & Retik, A. B. (2006). Tissue-engineered autologous bladders for patients needing cystoplasty. The Lancet, 367(9518), 1241–1246. doi:10.1016/s0140-6736(06)68438-9

Baker, B. M., & Chen, C. S. (2012). Deconstructing the third dimension: how 3D culture microenvironments alter cellular cues. J Cell Sci, 125(Pt 13), 3015-3024. doi:10.1242/jcs.079509

Biocompatibility Test Methods. Pacific BioLabs. (2018, September 18). Retrieved April 13, 2022, from https://pacificbiolabs.com/biocompatibility-test-methods

Blaeser, A., Duarte Campos, D. F., & Fischer, H. (2017). 3D bioprinting of cell-laden hydrogels for advanced tissue engineering. Current Opinion in Biomedical Engineering, 2, 58-66. doi: https://doi.org/10.1016/j.cobme.2017.04.003

Caliari, S. R., & Burdick, J. A. (2016). A practical guide to hydrogels for cell culture. Nature Methods, 13(5), 405-414. doi:10.1038/nmeth.3839

Chae, S., Hong, J., Hwangbo, H., & Kim, G. (2021). The utility of biomedical scaffolds laden with spheroids in various tissue engineering applications. Theranostics, 11(14), 6818–6832. doi:10.7150/thno.58421

Chen, M. H., Wang, L. L., Chung, J. J., Kim, Y.-H., Atluri, P., & Burdick, J. A. (2017). Methods To Assess Shear-Thinning Hydrogels for Application As Injectable Biomaterials. ACS Biomaterials Science & Engineering, 3(12), 3146–3160. doi:10.1021/acsbiomaterials.7b00734

Choe, S. S., Huh, J. Y., Hwang, I. J., Kim, J. I., & Kim, J. B. (2016). Adipose Tissue Remodeling: Its Role in Energy Metabolism and Metabolic Disorders. 7. doi:10.3389/fendo.2016.00030

Christensen, K., Xu, C., Chai, W., Zhang, Z., Fu, J., & Huang, Y. (2015). Freeform inkjet printing of cellular structures with bifurcations. Biotechnology and Bioengineering, 112(5), 1047–1055. doi:10.1002/bit.25501

Dai, X., Ma, C., Lan, Q., & Xu, T. (2016). 3D bioprinted glioma stem cells for brain tumor model and applications of drug susceptibility. Biofabrication, 8(4), 045005. doi:10.1088/1758-5090/8/4/045005

Darkes-Burkey, C., & Shepherd, R. F. (2020). High-resolution 3D printing in seconds. Nature, 588(7839), 594-595. doi:10.1038/d41586-020-03543-3

de Melo, B. A. G., Jodat, Y. A., Cruz, E. M., Benincasa, J. C., Shin, S. R., & Porcionatto, M. A. (2020). Strategies to use fibrinogen as bioink for 3D bioprinting fibrin-based soft and hard tissues. Acta Biomater, 117, 60-76. doi: 10.1016/j.actbio.2020.09.024

de Melo, B. A. G., Jodat, Y. A., Mehrotra, S., Calabrese, M. A., Kamperman, T., Mandal, B. B., . . . Shin, S. R. (2019). 3D Printed Cartilage-Like Tissue Constructs with Spatially Controlled Mechanical Properties. Advanced Functional Materials, 29(51), 1906330. doi:10.1002/adfm.201906330

Derakhshanfar, S., Mbeleck, R., Xu, K., Zhang, X., Zhong, W., Xing, M. (2018). 3D bioprinting for Biomedical Devices and tissue engineering: A review of recent trends and advances. Bioactive Materials, 3(2), 144–156. doi:10.1016/j.bioactmat.2017.11.008

Dhandayuthapani, B., Yoshida, Y., Maekawa, T., & Kumar, D. S. (2011). Polymeric Scaffolds in Tissue Engineering Application: A Review. International Journal of Polymer Science, 2011, 290602. doi:10.1155/2011/290602

Dinescu, S., Albu Kaya, M., Chitoiu, L., Ignat, S., Kaya, D. A., & Costache, M. (2018). Collagen-Based Hydrogels and Their Applications for Tissue Engineering and Regenerative Medicine. Polymers and Polymeric Composites: A Reference Series, 1–21. doi:10.1007/978-3-319-76573-0_54-1

Doering, L., Khatri, R., Petry, S. F., Sauer, H., Howaldt, H.-P., & Linn, T. (2019). Regulation of somatostatin expression by vitamin D3 and valproic acid in human adipose-derived mesenchymal stem cells. Stem Cell Research & Therapy, 10(1), 240. doi:10.1186/s13287-019-1330-x

El-Sherbiny, I. M., & Yacoub, M. H. (2013). Hydrogel scaffolds for tissue engineering: Progress and challenges. Global Cardiology Science and Practice, 2013(3), 38. doi:10.5339/gcsp.2013.38

Evans, N. D., Gentleman, E., & Polak, J. M. (2006). Scaffolds for stem cells. Materials Today, 9(12), 26–33. doi:10.1016/s1369-7021(06)71740-0

Finamore, T. A., Curtis, T. E., Tedesco, J. V., Grandfield, K., & Roeder, R. K. (2019). Nondestructive, longitudinal measurement of collagen scaffold degradation using computed tomography and gold nanoparticles. Nanoscale, 11(10), 4345–4354. doi:10.1039/c9nr00313d

Fitz-Gerald, J. M., Rack, P. D., Ringeisen, B., Young, D., Modi, R., Auyeung, R., & Wu, H.-D. (2002). Chapter 17 - Matrix Assisted Pulsed Laser Evaporation-Direct Write (Maple-Dw): A New Method to Rapidly Prototype Organic and Inorganic Materials. In A. Piqué (Ed.), Direct-Write Technologies for Rapid Prototyping (pp. 517-553). San Diego: Academic Press.

Freeman, F. E., & Kelly, D. J. (2017). Tuning Alginate Bioink Stiffness and Composition for Controlled Growth Factor Delivery and to Spatially Direct MSC Fate within Bioprinted Tissues. Scientific Reports, 7(1). doi:10.1038/s41598-017-17286-1

Gasperini, L., Mano, J. F., & Reis, R. L. (2014). Natural polymers for the microencapsulation of cells. Journal of The Royal Society Interface, 11(100), 20140817. doi:10.1098/rsif.2014.0817

Gentile, C. G. (2021). Printability, Durability, Contractility and Vascular Network Formation in 3D Bioprinted Cardiac Endothelial Cells Using Alginate–Gelatin Hydrogels. Frontiers in Bioengineering and Biotechnology, 9. doi:10.3389/fbioe.2021.636257

Gibas, I., & Janik, H. (2010). Review: Synthetic Polymer Hydrogels for Biomedical Applications. Chemistry & Chemical Technology, 4(4), 297–304. doi:10.23939/chcht04.04.297

Gomillion, C. T., & Burg, K. J. L. (2011). Adipose Tissue Engineering. Comprehensive Biomaterials, 529–539. doi:10.1016/b978-0-08-055294-1.00189-6

Gonzalez-Fernandez, T., Tenorio, A., Campbell, K., Silva, E., & Leach, J. K. (2020). Alginate-Based Bioinks for 3D Bioprinting and Fabrication of Anatomically Accurate Bone Grafts. Tissue Engineering Part A. doi:10.1089/ten.tea.2020.0305

Groll, J., Burdick, J. A., Cho, D.-W., Derby, B., Gelinsky, M., Heilshorn, S. C., . . . (2018). A definition of bioinks and their distinction from biomaterial inks. Biofabrication, 11(1), 013001. doi:10.1088/1758-5090/aaec52

Grzesiak, J., Kolankowski, J., & Marycz, K. (2015). Osteogenic Differentiation of Canine Adipose Stem Cells Cultured in Alginate-Fibrin-Based Hydrogel. Journal of Biomaterials and Tissue Engineering, 5(9), 703–710. doi:10.1166/jbt.2015.1366

Gyles, D. A., Castro, L. D., Silva, J. O., & Ribeiro-Costa, R. M. (2017). A review of the designs and prominent biomedical advances of natural and synthetic hydrogel formulations. European Polymer Journal, 88, 373–392. doi:10.1016/j.eurpolymj.2017.01.0270

Hinton Thomas, J., Jallerat, Q., Palchesko Rachelle, N., Park Joon, H., Grodzicki Martin, S., Shue, H.-J., . . (2015). Feinberg Adam, W. Three-dimensional printing of complex biological structures by freeform reversible embedding of suspended hydrogels. Science Advances, 1(9), e1500758. doi:10.1126/sciadv.1500758

Hong, L. T. A., Kim, Y.-M., Park, H. H., Hwang, D. H., Cui, Y., Lee, E. M., . . . Kim, B. G. (2017). An injectable hydrogel enhances tissue repair after spinal cord injury by promoting extracellular matrix remodelling. Nature Communications, 8(1), 533. doi:10.1038/s41467-017-00583-8

Hull, C.W. (1986). Apparatus for production of three-dimensional objects by stereolithography. US 4575330 A (Google Patents)

Huang, Y., He, K., & Wang, X. (2013). Rapid prototyping of a hybrid hierarchical polyurethane-cell/hydrogel construct for regenerative medicine. Materials Science and Engineering: C, 33(6), 3220–3229. doi:10.1016/j.msec.2013.03.048

Indurkar, A., Pandit, A., Jain, R., & Dandekar, P. (2020). Plant based cross-linkers for tissue engineering applications. Journal of Biomaterials Applications, 36(1), 76–94. doi:10.1177/0885328220979273

ISO - International Organization for Standardization. (2009). Biological evaluation of medical devices — Part 5: Tests for in vitro cytotoxicity. ISO 10993-5:2009. ISO. https://www.iso.org/standard/36406.html

Jakab, K., Neagu, A., Mironov, V., Markwald, R. R., & Forgacs, G. (2004). Engineering biological structures of prescribed shape using self-assembling multicellular systems. Proceedings of the National Academy of Sciences, 101(9), 2864–2869. doi:10.1073/pnas.0400164101

Jang, S., Boddorff, A., Jang, D. J., Lloyd, J., Wagner, K., Thadhani, N., & Brettmann, B. (2021). Effect of material extrusion process parameters on filament geometry and inter-filament voids in as-fabricated high solids loaded polymer composites. Additive Manufacturing, 47, 102313. doi:10.1016/j.addma.2021.102313

Jia, W., Gungor-Ozkerim, P. S., Zhang, Y. S., Yue, K., Zhu, K., Liu, W., Pi, Q., Byambaa, B., Dokmeci, M. R., Shin, S. R., & Khademhosseini, A. (2016). Direct 3D bioprinting of perfusable vascular constructs using a blend bioink. Biomaterials, 106, 58–68. doi:10.1016/j.biomaterials.2016.07.038

Joosten, E. A., Veldhuis, W. B., & Hamers, F. P. (2004). Collagen containing neonatal astrocytes stimulates regrowth of injured fibers and promotes modest locomotor recovery after spinal cord injury. J Neurosci Res, 77(1), 127-142. doi:10.1002/jnr.20088

Lueckgen, A., Garske, D. S., Ellinghaus, A., Mooney, D. J., Duda, G. N., & Cipitria, A. (2019). Enzymatically-degradable alginate hydrogels promote cell spreading and in vivo tissue infiltration. Biomaterials, 217, 119294. doi:10.1016/j.biomaterials.2019.119294

Kampschulte, M., Langheinirch, A. C., Sender, J., Litzlbauer, H. D., Althöhn, U., Schwab, J. D,. Krombach, G. A. (2016). Nano-Computed Tomography: Technique and Applications. Rofo, 188(2), 146-154. doi:10.1055/s-0041-106541

Kaphalia, B. S. (2014). Chapter 16 - Biomarkers of acute and chronic pancreatitis. In R. C. Gupta (Ed.), Biomarkers in Toxicology (pp. 279-289). Boston: Academic Press.

Kaveh, M., Badrossamay, M., Foroozmehr, E., & Hemasian Etefagh, A. (2015). Optimization of the printing parameters affecting dimensional accuracy and internal cavity for HIPS material used in fused deposition modeling processes. Journal of Materials Processing Technology, 226, 280–286. doi:10.1016/j.jmatprotec.2015.07.012

Kisiday, J. D., Hale, B. W., Almodovar, J. L., Lee, C. M., Kipper, M. J., Wayne McIlwraith, C., & Frisbie, D. D. (2011). Expansion of mesenchymal stem cells on fibrinogen-rich protein surfaces derived from blood plasma. J Tissue Eng Regen Med, 5(8), 600-611. doi:10.1002/term.352

Landers, R., Hübner, U., Schmelzeisen, R., & Mülhaupt, R. (2002). Rapid prototyping of scaffolds derived from thermoreversible hydrogels and tailored for applications in tissue engineering. Biomaterials, 23(23), 4437–4447. doi:10.1016/s0142-9612(02)00139-4

Laurens, N., Koolwijk, P., & De Maat, M. P. M. (2006). Fibrin structure and wound healing. Journal of Thrombosis and Haemostasis, 4(5), 932-939. doi:10.1111/j.1538-7836.2006.01861.x

Leberfinger, A. N., Ravnic, D. J., Dhawan, A., & Ozbolat, I. T. (2017). Concise Review: Bioprinting of Stem Cells for Transplantable Tissue Fabrication. STEM CELLS Translational Medicine, 6(10), 1940–1948. *doi:10.1002/sctm.17-0148*

Lee, C. H., Singla, A., & Lee, Y. (2001). Biomedical applications of collagen. Int J Pharm, 221(1-2), 1-22. doi:10.1016/s0378-5173(01)00691-3

Lee, J., Song, B., Subbiah, R., Chung, J. J., Choi, U. H., Park, K., . . . Oh, S. J. (2019). Effect of chain flexibility on cell adhesion: Semi-flexible model-based analysis of cell adhesion to hydrogels. Sci Rep, 9(1), 2463. doi:10.1038/s41598-019-38951-7

Lee, K. Y., & Mooney, D. J. (2012). Alginate: Properties and biomedical applications. Progress in Polymer Science, 37(1), 106–126. *doi:*10.1016/j.progpolymsci.2011.06.003

Li, R., Liu, J., Ma, J., Sun, X., Wang, Y., Yan, J., Yu, Q., Diao, J., Yang, C., Reid, L. M., & Wang, Y. (2022). Fibrinogen improves liver function via promoting cell aggregation and fibronectin assembly in hepatic spheroids. Biomaterials, 280, 121266. doi:10.1016/j.biomaterials.2021.121266

Li, S., Yan, Y., Xiong, Z., Zhang, C. W. R., & Wang, X. (2009). Gradient Hydrogel Construct Based on an Improved Cell Assembling System. Journal of Bioactive and Compatible Polymers, 24(1_suppl), 84–99. doi:10.1177/0883911509103357

Li S., Xiong Z., Wang X., Yan Y., Liu H., & Zhang R. (2009). Direct Fabrication of a Hybrid Cell/Hydrogel Construct by a Double-nozzle Assembling Technology. Journal of Bioactive and Compatible Polymers, 24(3), 249–265. doi:10.1177/0883911509104094

Liu, S. Q., Tian, Q., Hedrick, J. L., Po Hui, J. H., Ee, P. L., & Yang, Y. Y. (2010). Biomimetic hydrogels for chondrogenic differentiation of human mesenchymal stem cells to neocartilage. Biomaterials, 31(28), 7298-7307. doi:10.1016/j.biomaterials.2010.06.001

Live/DEAD™ viability/cytotoxicity kit, for mammalian cells. Thermo Fisher Scientific - US. (n.d.). Retrieved April 12, 2022, from https://www.thermofisher.com/order/catalog/product/L3224

Madl, C. M., Katz, L. M., & Heilshorn, S. C. (2018). Tuning Bulk Hydrogel Degradation by Simultaneous Control of Proteolytic Cleavage Kinetics and Hydrogel Network Architecture. ACS Macro Letters, 7(11), 1302-1307. doi:10.1021/acsmacrolett.8b00664

Maitra, J., & Shukla, V. K. (2014). Cross-linking in Hydrogels - A Review. American Journal of Polymer Science. 4(2), 25-31. doi:10.5923/j.ajps.20140402.01

Mishra, M. K. (2015). Encyclopedia of biomedical polymers and polymeric biomaterials. Crc Press/Taylor & Francis Group.

Montalbano, G., Toumpaniari, S., Popov, A., Duan, P., Chen, J., Dalgarno, K., Scott, W. E., & Ferreira, A. M. (2018). Synthesis of bioinspired collagen/alginate/fibrin based hydrogels for soft tissue engineering. Materials Science and Engineering: C, 91, 236–246. doi:10.1016/j.msec.2018.04.101

Montgomery, A., Wong, A., Gabers, N., & Willerth, S. M. (2015). Engineering personalized neural tissue by combining induced pluripotent stem cells with fibrin scaffolds. Biomaterials Science, 3(2), 401-413. doi:10.1039/C4BM00299G

Mosmann, T. (1983). Rapid colorimetric assay for cellular growth and survival: application to proliferation and cytotoxicity assays. J Immunol Methods, 65(1-2), 55-63. doi:10.1016/0022-1759(83)90303-4

Mostafaeie A., Elliott A. M., Barnes J. E., Li F., Tan W., Cramer C. L., Nandwana P., Chmielus M. (2021) Binder jet 3D printing – Process parameters, materials, properties, and challenges.. Progress in Materials Science, 119. doi:10.1016/j.pmatsci.2020.100707

Murphy, S. V., & Atala, A. (2014). 3D bioprinting of tissues and organs. Nature Biotechnology, 32(8), 773-785. doi:10.1038/nbt.2958

Naahidi, S., Jafari, M., Logan, M., Wang, Y., Yuan, Y., Bae, H., . . . Chen, P. (2017). Biocompatibility of hydrogel-based scaffolds for tissue engineering applications. Biotechnol Adv, 35(5), 530-544. doi:10.1016/j.biotechadv.2017.05.006

Nakamura, M., Iwanaga, S., Henmi, C., Arai, K., & Nishiyama, Y. (2010). Biomatrices and biomaterials for future developments of bioprinting and biofabrication. Biofabrication, 2(1), 014110. doi:10.1088/1758-5082/2/1/014110

Ning, L., Sun, H., Lelong, T., Guilloteau, R., Zhu, N., Schreyer, D. J., & Chen, X. (2018). 3D bioprinting of scaffolds with living Schwann cells for potential nerve tissue engineering applications. Biofabrication, 10(3), 035014. doi:10.1088/1758-5090/aacd30

Organ Donation Statistics | organdonor.gov. [online], 2022 Available at: https://www.organdonor.gov/learn/organ-donation-statistics [Accessed 15 April 2022].

Ozeki, M., & Tabata, Y. (2005). In vivo degradability of hydrogels prepared from different gelatins by various cross-linking methods. Journal of Biomaterials Science, Polymer Edition, 16(5), 549–561. doi:10.1163/1568562053783731

Pellegrino, A. (2021). Duquesne Scholarship Collection Duquesne Scholarship Collection Bioprinting Alginate Structures using the FRESH Method Bioprinting Alginate Structures using the FRESH Method. https://dsc.duq.edu/cgi/viewcontent.cgi?article=1063&context=urss

Peña, B., Laughter, M., Jett, S., Rowland, T. J., Taylor, M. R., Mestroni, L., & Park, D. (2018). Injectable hydrogels for cardiac tissue engineering. Macromolecular Bioscience, 18(6), 1800079. doi:10.1002/mabi.201800079

Qin, Y. (2003). Gel swelling properties of alginate fibers. Journal of Applied Polymer Science, 91(3), 1641–1645. doi:10.1002/app.13317

Ramakrishnan, R., Kasoju, N., Raju, R., Geevarghese, R., Gauthaman, A., & Bhatt, A. (2022). Exploring the Potential of Alginate-Gelatin-Diethylaminoethyl Cellulose-Fibrinogen based Bioink for 3D Bioprinting of Skin Tissue Constructs. Carbohydrate Polymer Technologies and Applications, 3, 100184. doi:10.1016/j.carpta.2022.100184

Rana, D., Kumar, T. S., & Ramalingam, M. (2014). Cell-laden hydrogels for tissue engineering. Journal of Biomaterials and Tissue Engineering, 4(7), 507–535. doi:10.1166/jbt.2014.1206

Ravindranath, M. H., El Hilali, F., & Filippone, E. J. (2021). The Impact of Inflammation on the Immune Responses to Transplantation: Tolerance or Rejection? Frontiers in Immunology, 12. doi:10.3389/fimmu.2021.667834

Rutz, A. L., Hyland, K. E., Jakus, A. E., Burghardt, W. R., & Shah, R. N. (2015). A multimaterial bioink method for 3D printing tunable, cell-compatible hydrogels. Adv Mater, 27(9), 1607-1614. doi:10.1002/adma.201405076

Salamon, A., van Vlierberghe, S., van Nieuwenhove, I., Baudisch, F., Graulus, G.-J., Benecke, V., . . . Peters, K. (2014). Gelatin-Based Hydrogels Promote Chondrogenic Differentiation of Human Adipose Tissue-Derived Mesenchymal Stem Cells In Vitro. Materials (Basel, Switzerland), 7(2), 1342-1359. doi:10.3390/ma7021342

Saroia, J., Yanen, W., Wei, Q., Zhang, K., Lu, T., & Zhang, B. (2018). A review on biocompatibility nature of hydrogels with 3D printing techniques, tissue engineering application and its future prospective. Bio-Design and Manufacturing, 1(4), 265-279. doi:10.1007/s42242-018-0029-7

Schöneberg, J., De Lorenzi, F., Theek, B., Blaeser, A., Rommel, D., Kuehne, A. J. C., . . . Fischer, H. (2018). Engineering biofunctional in vitro vessel models using a multilayer bioprinting technique. Sci Rep, 8(1), 10430. doi:10.1038/s41598-018-28715-0

Shamblott, M. J., Axelman, J., Wang, S., Bugg, E. M., Littlefield, J. W., Donovan, P. J., Blumenthal, P. D., Huggins, G. R., & Gearhart, J. D. (1998). Derivation of pluripotent stem cells from cultured human primordial germ cells. Proceedings of the National Academy of Sciences, 95(23), 13726–13731. doi:10.1073/pnas.95.23.13726

Shiwarski, D. J., Hudson, A. R., Tashman, J. W., & Feinberg, A. W. (2021). Emergence of FRESH 3D printing as a platform for advanced tissue biofabrication. APL bioengineering, 5(1), 010904-010904. doi:10.1063/5.0032777

Singh, T. R. R., McMillan, H., Mooney, K., Alkilani, A. Z., & Donnelly, R. F. (2013). 6 - Microneedles for drug delivery and monitoring. In X. Li & Y. Zhou (Eds.), Microfluidic Devices for Biomedical Applications (pp. 185-230): Woodhead Publishing.

Siqi Du, X. Z. (2015). Anti-Cancer Drug Screening Based on a Adipose-Derived Stem Cell/Hepatocyte 3D Printing Technique. Journal of Stem Cell Research & Therapy, 05(04). doi:10.4172/2157-7633.1000273

Siti Ibrahim, S. F., Mohd Azam, N. A., & Mat Amin, K. A. (2019). Sodium alginate film: The effect of Crosslinker on physical and mechanical properties. IOP Conference Series: Materials Science and Engineering, 509, 012063. doi:10.1088/1757-899x/509/1/012063

Snyder, T. N., Madhavan, K., Intrator, M., Dregalla, R. C., & Park, D. (2014). A fibrin/hyaluronic acid hydrogel for the delivery of mesenchymal stem cells and potential for articular cartilage repair. Journal of Biological Engineering, 8(1). doi:10.1186/1754-1611-8-10zhang

Song, F., Gong, J., Tao, Y., Cheng, Y., Lu, J., & Wang, H. (2021). A robust regenerated cellulose-based dual stimuli-responsive hydrogel as an intelligent switch for controlled drug delivery. International Journal of Biological Macromolecules, 176, 448–458. doi:10.1016/j.ijbiomac.2021.02.104

Sproul, E., Nandi, S., & Brown, A. (2018). Fibrin biomaterials for tissue regeneration and repair. Peptides and Proteins as Biomaterials for Tissue Regeneration and Repair, 151–173. doi:10.1016/b978-0-08-100803-4.00006-1

Sriphutkiat, Y., Kasetsirikul, S., Ketpun, D., & Zhou, Y. (2019). Cell alignment and accumulation using acoustic nozzle for bioprinting. Sci Rep, 9(1), 17774. doi:10.1038/s41598-019-54330-8

Strober, W. (2015). Trypan Blue Exclusion Test of cell viability. Current Protocols in Immunology, 111(1). doi:10.1002/0471142735.ima03bs111

Su, Y., Denbeigh, J. M., Camilleri, E. T., Riester, S. M., Parry, J. A., Wagner, E. R., Yaszemski, M. J., Dietz, A. B., Cool, S. M., van Wijnen, A. J., & Kakar, S. (2018). Extracellular matrix protein production in human adipose-derived mesenchymal stem cells on three-dimensional polycaprolactone (PCL) scaffolds responds to GDF5 or FGF2. Gene Reports, 10, 149–156. doi:10.1016/j.genrep.2017.12.004

Swain, S. K., & Sarkar, D. (2014). Fabrication, bioactivity, in vitro cytotoxicity and cell viability of cryo-treated nanohydroxyapatite–gelatin–polyvinyl alcohol macroporous scaffold. Journal of Asian Ceramic Societies, 2(3), 241-247. doi: doi:10.1016/j.jascer.2014.05.003

Tangsadthakun, C., Kanokpanont, S., Sanchavanakit, N., Banaprasert, T., & Damrongsakkul, S. (2017). Properties of collagen/chitosan scaffolds for skin tissue engineering. Journal of Metals, Materials and Minerals, 16(1).

ThelwelL, C., & Longstaff, C. (2007). The regulation by fibrinogen and fibrin of tissue plasminogen activator kinetics and inhibition by plasminogen activator inhibitor 1. Journal of Thrombosis and Haemostasis, 5(4), 804–811. doi:10.1111/j.1538-7836.2007.02422.x

Theocharis, A. D., Skandalis, S. S., Gialeli, C., & Karamanos, N. K. (2016). Extracellular matrix structure. Advanced Drug Delivery Reviews, 97, 4-27. doi:10.1016/j.addr.2015.11.001

Thomas, A. (2000). Alginates from wound dressings activate human macrophages to secrete tumour necrosis factor-α. Biomaterials, 21(17), 1797–1802. doi:10.1016/s0142-9612(00)00072-7

Tibbitt, M. W., & Anseth, K. S. (2009). Hydrogels as extracellular matrix mimics for 3D cell culture. Biotechnol Bioeng, 103(4), 655-663. doi:10.1002/bit.22361

Tse, C., Whiteley, R., Yu, T., Stringer, J., MacNeil, S., Haycock, J. W., & Smith, P. J. (2016). Inkjet printing Schwann cells and neuronal analogue NG108-15 cells. Biofabrication, 8(1), 015017. doi:10.1088/1758-5090/8/1/015017

Verheijen, M., Lienhard, M., Schrooders, Y., Clayton, O., Nudischer, R., Boerno, S., Timmermann, B., Selevsek, N., Schlapbach, R., Gmuender, H., Gotta, S., Geraedts, J., Herwig, R., Kleinjans, J., & Caiment, F. (2019). DMSO induces drastic changes in human cellular processes and epigenetic landscape in vitro. Scientific Reports, 9(1). doi:10.1038/s41598-019-40660-0

Vitaprint Platforma. Institute IRNAS. (n.d.). Retrieved April 19, 2022, from https://www.irnas.eu/sl/vitaprint-platforma/

Walker, C. P., & Royston, D. (2002). Thrombin generation and its inhibition: a review of the scientific basis and mechanism of action of anticoagulant therapies. Br J Anaesth, 88(6), 848-863. doi:10.1093/bja/88.6.848

Walles, H., & Walles, T. (2011). Extracellular matrix as biomimetic biomaterial: Biological matrices for tissue regeneration. *Comprehensive Biomaterials*, 361–367. doi:10.1016/b978-0-08-055294-1.00077-5

Wang, J., Liu, Y., Zhang, X., Rahman, S., Su, S., Wei, J., Ning, F., Hu, Z., Martínez-Zaguilán, R., Sennoune, S., Cong, W., Christopher, G., Zhang, K. and Qiu, J., (2021). 3D printed agar/ calcium alginate hydrogels with high shape fidelity and tailorable mechanical properties. Polymer, 214, p.123238. doi:10.1016/j.polymer.2020.123238

Wang, X., Li, X., Dai, X., Zhang, X., Zhang, J., Xu, T., & Lan, Q. (2018). Bioprinting of glioma stem cells improves their endotheliogenic potential. Colloids and Surfaces B: Biointerfaces, 171, 629–637. doi:10.1016/j.colsurfb.2018.08.006

Wang, X., Zhao, X., Zhou, X., & Liu, C. (2016). A 3D bioprinting liver tumor model for drug screening. Semantic Scholar. doi:10.20959/WJPPS20164-6311

Wichterle, O., & Lim, D. (1960). Hydrophilic Gels for Biological Use. Nature, 185(4706), 117-118. doi:10.1038/185117a0

Xradia 610 & 620 Versa. (n.d.). Www.zeiss.com. Retrieved May 17, 2022, from https://www.zeiss.com/microscopy/int/products/x-ray-microscopy/zeiss-xradia-610-and-620-versa.html

Xu, M., Van, Y., Liu, H., Yag, R., & Wang, X. (2009). Controlled Adipose-derived Stromal Cells Differentiation into Adipose and Endothelial Cells in a 3D Structure Established by Cell-assembly Technique. Journal of Bioactive and Compatible Polymers, 24(1_suppl), 31–47. doi:10.1177/0883911509102794

Xu, T., Jin, J., Gregory, C., Hickman, J. J., & Boland, T. (2005). Inkjet printing of viable mammalian cells. Biomaterials, 26(1), 93-99. doi:10.1016/j.biomaterials.2004.04.011

Zhang, Y. S., Arneri, A., Bersini, S., Shin, S.-R., Zhu, K., Goli-Malekabadi, Z., . . . (2016). Bioprinting 3D microfibrous scaffolds for engineering endothelialized myocardium and heart-on-a-chip. Biomaterials, 110, 45–59. doi:10.1016/j.biomaterials.2016.09.003

Zhao, Y., Yao, R., Ouyang, L., Ding, H., Zhang, T., Zhang, K., Cheng, S., & Sun, W. (2014). Three-dimensional printing of Hela cells for cervical tumor model in vitro. Biofabrication, 6(3), 035001. doi:10.1088/1758-5082/6/3/035001

Zopf, D. A., Hollister, S. J., Nelson, M. E., Ohye, R. G., & Green, G. E. (2013). Bioresorbable Airway Splint Created with a Three-Dimensional Printer. New England Journal of Medicine, 368(21), 2043-2045. doi:10.1056/NEJMc1206319

APPENDIX

G-code for 3D printing the scaffolds

```
G92X0    Y0
G1 Z0    F500.0

G1 A[#<_a> +0.05] ;ramp

G1 X10.0 Y0.0  A[#<_a> +0.2* #<_hw_jogpot>/511]
G1 X10.0 Y1.25 A[#<_a> +0.025* #<_hw_jogpot>/511]
G1 X0.0  Y1.25 A[#<_a> +0.2* #<_hw_jogpot>/511]
G1 X0.0  Y2.5  A[#<_a> +0.025* #<_hw_jogpot>/511]
G1 X10.0 Y2.5  A[#<_a> +0.2* #<_hw_jogpot>/511]
G1 X10.0 Y3.75 A[#<_a> +0.025* #<_hw_jogpot>/511]
G1 X0.0  Y3.75 A[#<_a> +0.2* #<_hw_jogpot>/511]
G1 X0.0  Y5.0  A[#<_a> +0.025* #<_hw_jogpot>/511]
G1 X10.0 Y5.0  A[#<_a> +0.2* #<_hw_jogpot>/511]
G1 X10.0 Y6.25 A[#<_a> +0.025* #<_hw_jogpot>/511]
G1 X0.0  Y6.25 A[#<_a> +0.2* #<_hw_jogpot>/511]
G1 X0.0  Y7.5  A[#<_a> +0.025* #<_hw_jogpot>/511]
G1 X10.0 Y7.5  A[#<_a> +0.2* #<_hw_jogpot>/511]
G1 X10.0 Y8.75 A[#<_a> +0.025* #<_hw_jogpot>/511]
G1 X0.0  Y8.75 A[#<_a> +0.2* #<_hw_jogpot>/511]
G1 X0.0  Y10.0 A[#<_a> +0.025* #<_hw_jogpot>/511]
G1 X10.0 Y10.0 A[#<_a> +0.2* #<_hw_jogpot>/511]

G1 Z[#<_z> +0.2]

G1 X10.0 Y0.0  A[#<_a> +0.2* #<_hw_jogpot>/511]
G1 X8.75 Y0.0  A[#<_a> +0.025* #<_hw_jogpot>/511]
G1 X8.75 Y10.0 A[#<_a> +0.2* #<_hw_jogpot>/511]
G1 X7.5  Y10.0 A[#<_a> +0.025* #<_hw_jogpot>/511]
G1 X7.5  Y0.0  A[#<_a> +0.2* #<_hw_jogpot>/511]
G1 X6.25 Y0.0  A[#<_a> +0.025* #<_hw_jogpot>/511]
G1 X6.25 Y10.0 A[#<_a> +0.2* #<_hw_jogpot>/511]
G1 X5.0  Y10.0 A[#<_a> +0.025* #<_hw_jogpot>/511]
G1 X5.0  Y0.0  A[#<_a> +0.2* #<_hw_jogpot>/511]
G1 X3.75 Y0.0  A[#<_a> +0.025* #<_hw_jogpot>/511]
G1 X3.75 Y10.0 A[#<_a> +0.2* #<_hw_jogpot>/511]
G1 X2.5  Y10.0 A[#<_a> +0.025* #<_hw_jogpot>/511]
G1 X2.5  Y0.0  A[#<_a> +0.2* #<_hw_jogpot>/511]
G1 X1.25 Y0.0  A[#<_a> +0.025* #<_hw_jogpot>/511]
G1 X1.25 Y10.0 A[#<_a> +0.2* #<_hw_jogpot>/511]
G1 X0.0  Y10.0 A[#<_a> +0.025* #<_hw_jogpot>/511]
G1 X0.0  Y0.0  A[#<_a> +0.2* #<_hw_jogpot>/511]

G1 Z[#<_z> +0.2]

G1 X10.0 Y0.0  A[#<_a> +0.2* #<_hw_jogpot>/511]
G1 X10.0 Y1.25 A[#<_a> +0.025* #<_hw_jogpot>/511]
G1 X0.0  Y1.25 A[#<_a> +0.2* #<_hw_jogpot>/511]
G1 X0.0  Y2.5  A[#<_a> +0.025* #<_hw_jogpot>/511]
G1 X10.0 Y2.5  A[#<_a> +0.2* #<_hw_jogpot>/511]
G1 X10.0 Y3.75 A[#<_a> +0.025* #<_hw_jogpot>/511]
G1 X0.0  Y3.75 A[#<_a> +0.2* #<_hw_jogpot>/511]
G1 X0.0  Y5.0  A[#<_a> +0.025* #<_hw_jogpot>/511]
```

```
G1 X10.0 Y5.0  A[#<_a> +0.2* #<_hw_jogpot>/511]
G1 X10.0 Y6.25 A[#<_a> +0.025* #<_hw_jogpot>/511]
G1 X0.0  Y6.25 A[#<_a> +0.2* #<_hw_jogpot>/511]
G1 X0.0  Y7.5  A[#<_a> +0.025* #<_hw_jogpot>/511]
G1 X10.0 Y7.5  A[#<_a> +0.2* #<_hw_jogpot>/511]
G1 X10.0 Y8.75 A[#<_a> +0.025* #<_hw_jogpot>/511]
G1 X0.0  Y8.75 A[#<_a> +0.2* #<_hw_jogpot>/511]
G1 X0.0  Y10.0 A[#<_a> +0.025* #<_hw_jogpot>/511]
G1 X10.0 Y10.0 A[#<_a> +0.2* #<_hw_jogpot>/511]

G1 Z[#<_z> +0.2]

G1 X10.0 Y0.0  A[#<_a> +0.2* #<_hw_jogpot>/511]
G1 X8.75 Y0.0  A[#<_a> +0.025* #<_hw_jogpot>/511]
G1 X8.75 Y10.0 A[#<_a> +0.2* #<_hw_jogpot>/511]
G1 X7.5  Y10.0 A[#<_a> +0.025* #<_hw_jogpot>/511]
G1 X7.5  Y0.0  A[#<_a> +0.2* #<_hw_jogpot>/511]
G1 X6.25 Y0.0  A[#<_a> +0.025* #<_hw_jogpot>/511]
G1 X6.25 Y10.0 A[#<_a> +0.2* #<_hw_jogpot>/511]
G1 X5.0  Y10.0 A[#<_a> +0.025* #<_hw_jogpot>/511]
G1 X5.0  Y0.0  A[#<_a> +0.2* #<_hw_jogpot>/511]
G1 X3.75 Y0.0  A[#<_a> +0.025* #<_hw_jogpot>/511]
G1 X3.75 Y10.0 A[#<_a> +0.2* #<_hw_jogpot>/511]
G1 X2.5  Y10.0 A[#<_a> +0.025* #<_hw_jogpot>/511]
G1 X2.5  Y0.0  A[#<_a> +0.2* #<_hw_jogpot>/511]
G1 X1.25 Y0.0  A[#<_a> +0.025* #<_hw_jogpot>/511]
G1 X1.25 Y10.0 A[#<_a> +0.2* #<_hw_jogpot>/511]
G1 X0.0  Y10.0 A[#<_a> +0.025* #<_hw_jogpot>/511]
G1 X0.0  Y0.0  A[#<_a> +0.2* #<_hw_jogpot>/511]

G1 Z[#<_z> +0.2]

G1 X10.0 Y0.0  A[#<_a> +0.2* #<_hw_jogpot>/511]
G1 X10.0 Y1.25 A[#<_a> +0.025* #<_hw_jogpot>/511]
G1 X0.0  Y1.25 A[#<_a> +0.2* #<_hw_jogpot>/511]
G1 X0.0  Y2.5  A[#<_a> +0.025* #<_hw_jogpot>/511]
G1 X10.0 Y2.5  A[#<_a> +0.2* #<_hw_jogpot>/511]
G1 X10.0 Y3.75 A[#<_a> +0.025* #<_hw_jogpot>/511]
G1 X0.0  Y3.75 A[#<_a> +0.2* #<_hw_jogpot>/511]
G1 X0.0  Y5.0  A[#<_a> +0.025* #<_hw_jogpot>/511]
G1 X10.0 Y5.0  A[#<_a> +0.2* #<_hw_jogpot>/511]
G1 X10.0 Y6.25 A[#<_a> +0.025* #<_hw_jogpot>/511]
G1 X0.0  Y6.25 A[#<_a> +0.2* #<_hw_jogpot>/511]
G1 X0.0  Y7.5  A[#<_a> +0.025* #<_hw_jogpot>/511]
G1 X10.0 Y7.5  A[#<_a> +0.2* #<_hw_jogpot>/511]
G1 X10.0 Y8.75 A[#<_a> +0.025* #<_hw_jogpot>/511]
G1 X0.0  Y8.75 A[#<_a> +0.2* #<_hw_jogpot>/511]
G1 X0.0  Y10.0 A[#<_a> +0.025* #<_hw_jogpot>/511]
G1 X10.0 Y10.0 A[#<_a> +0.2* #<_hw_jogpot>/511]

G1 Z[#<_z> +0.2]

G1 A[#<_a> -0.05] ;retract
G1 Z[#<_z> +2] ;go to safe height
G1 X15.0 Y0 ;go to next xy position
```

Plate organization for Alamar Blue assay

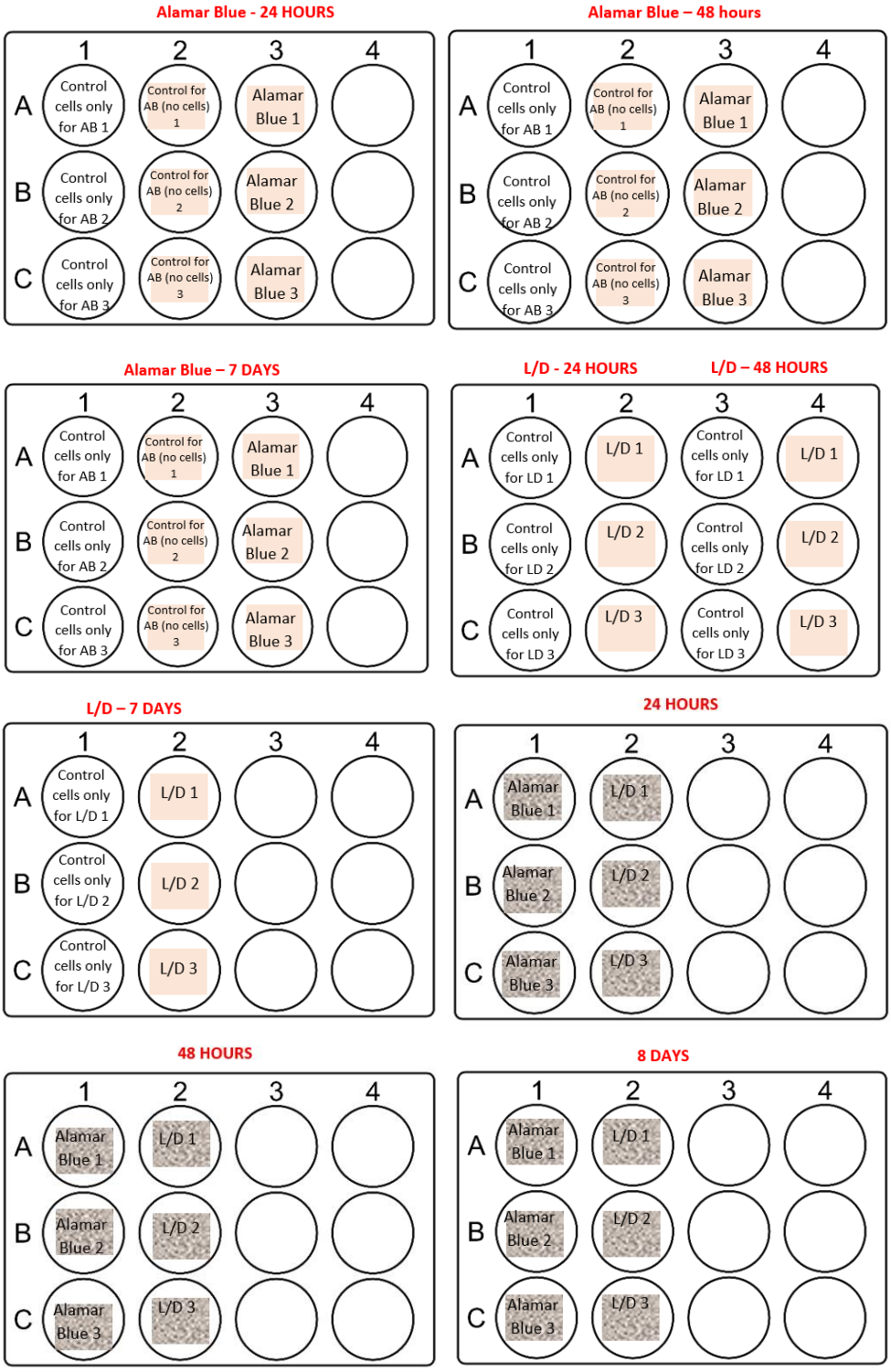

Figure 17. 24-well plate organization for Alamar Blue experiments at different time points. L/D refers to Live/Dead assay and the soft orange squares represent the scaffolds made of ink only, whereas the dotted orange squares represent bioink scaffolds. Each experiment was performed in triplicates.